

# The F-box protein UFO controls flower development by redirecting the master transcription factor LEAFY to new *cis*-elements

Received: 18 August 2022

Accepted: 20 December 2022

Published online: 2 February 2023

Philippe Rieu<sup>1</sup>, Laura Turchi<sup>1,2</sup>, Emmanuel Thévenon<sup>1</sup>, Eleftherios Zarkadas<sup>3,4</sup>, Max Nanao<sup>5</sup>, Hicham Chahtane<sup>1,6</sup>, Gabrielle Tichtinsky<sup>1</sup>, Jérémie Lucas<sup>1</sup>, Romain Blanc-Mathieu<sup>1</sup>, Chloe Zubieta<sup>1</sup>, Guy Schoehn<sup>1,6</sup> & François Parcy<sup>1</sup>✉

 Check for updates

In angiosperms, flower development requires the combined action of the transcription factor LEAFY (LFY) and the ubiquitin ligase adaptor F-box protein, UNUSUAL FLORAL ORGANS (UFO), but the molecular mechanism underlying this synergy has remained unknown. Here we show in transient assays and stable transgenic plants that the connection to ubiquitination pathways suggested by the UFO F-box domain is mostly dispensable.

On the basis of biochemical and genome-wide studies, we establish that UFO instead acts by forming an active transcriptional complex with LFY at newly discovered regulatory elements. Structural characterization of the LFY–UFO–DNA complex by cryo-electron microscopy further demonstrates that UFO performs this function by directly interacting with both LFY and DNA. Finally, we propose that this complex might have a deep evolutionary origin, largely predating flowering plants. This work reveals a unique mechanism of an F-box protein directly modulating the DNA binding specificity of a master transcription factor.

The formation of flowers is key to the reproductive success of angiosperms. Flowers are made of four types of organs (sepals, petals, stamens and carpels) arranged in concentric whorls. The patterning of flower meristems requires the localized induction of the ABCE floral homeotic genes that determine specific floral organ identities. In *Arabidopsis thaliana*, this developmental step is largely controlled by the master transcription factor (TF) LEAFY (LFY) that activates the ABCE genes<sup>1,2</sup>. LFY directly activates the A class gene *APETALA1* (*API*) uniformly in the early flower meristem<sup>3,4</sup>, while activations of B and C

genes are local and require the activity of cofactors. For instance, LFY regulates the C class gene *AGAMOUS* (*AG*) in conjunction with the TF WUSCHEL to specify third whorl (stamen) and fourth whorl (carpel) identities<sup>5</sup>. The activation of the B class gene *APETALA3* (*AP3*), necessary to specify the identity of the second (petal) and third whorls of the flower, requires the combined activity of LFY and the spatially delineated cofactor UNUSUAL FLORAL ORGANS (UFO)<sup>6–8</sup>. In *Arabidopsis*, the main function of LFY and UFO is to activate *AP3* (ref. <sup>9</sup>), but in numerous species (such as rice, wheat, tomato and petunia), their joint role

<sup>1</sup>Laboratoire Physiologie Cellulaire et Végétale, IRIG-DBSCI-LPCV, Université Grenoble Alpes, CEA, CNRS, INRAE, Grenoble, France. <sup>2</sup>Translational

Innovation in Medicine and Complexity, Université Grenoble Alpes, CNRS, Grenoble, France. <sup>3</sup>IBS, Université Grenoble Alpes, CNRS, CEA, Grenoble, France. <sup>4</sup>EMBL, ISBG, Université Grenoble Alpes, CNRS, CEA, Grenoble, France. <sup>5</sup>Structural Biology Group, European Synchrotron Radiation Facility, Grenoble, France. <sup>6</sup>Present address: Green Mission Pierre Fabre, Conservatoire Botanique Pierre Fabre, Institut de Recherche Pierre Fabre, Soual, France.

✉e-mail: [francois.parcy@cea.fr](mailto:francois.parcy@cea.fr)

goes well beyond B gene activation and is key to floral meristem and inflorescence development<sup>10–13</sup>.

At the molecular level, little is known on the nature of LFY–UFO synergy. Unlike most floral regulators, *UFO* encodes not for a TF but for an F-box protein, one of the first to be described in plants<sup>14–16</sup>. *UFO* is part of a SKP1–Cullin1–F-box (SCF) E3 ubiquitin ligase complex through the interaction of its F-box domain with ARABIDOPSIS SKP1-LIKE (ASK) proteins<sup>15,17</sup>. In addition, its predicted carboxy-terminal Kelch-type β-propeller domain physically interacts with LFY DNA Binding Domain (DBD)<sup>18</sup>. As the control of TF activity through proteolytic and non-proteolytic ubiquitination is a well-described mechanism<sup>19</sup>, it has been suggested that LFY is targeted for ubiquitination and possibly degradation by the SCF<sup>UFO</sup> complex. Other data have shown that adding a repression or activation domain to *UFO* changes its activity and that *UFO* is recruited at the *AP3* promoter in a LFY-dependent manner, suggesting a more direct role of *UFO* in gene regulation<sup>18,20</sup>. However, direct evidence explaining how *UFO* regulates a specific subset of LFY targets was still missing, and the molecular mechanism underlying LFY–UFO synergistic action remained elusive.

Here we show that the connection of *UFO* to the SCF complex is largely dispensable for this protein's activity and that an important role of *UFO* is to form a transcriptional complex with LFY at genomic sites devoid of canonical high-affinity LFY binding sites (LFYBS). Our study presents a unique mechanism by which an F-box protein acts as an integral part of a transcriptional complex.

## The *UFO* F-box domain is partially dispensable for its floral role

A dual luciferase reporter assay (DLRA) in *Arabidopsis* protoplasts was used to study floral promoter activation by LFY and *UFO*. We used promoter versions known to allow full complementation of mutants or to be able to recapitulate a wild-type (WT) expression pattern (Methods). We found that the *AP3* promoter (*pAP3*) was more strongly activated when LFY (or LFY–VP16, a fusion of LFY with the VP16 activation domain) was co-expressed with *UFO* (or *UFO*–VP16) than by either effector alone (Fig. 1a,e). Similar results were obtained with the promoter of *RABBIT EARS* (*RBE*), another *UFO* target (Fig. 1b)<sup>21</sup>. We also analysed the promoters of *API* (*pAPI*) and *AG* (*pAG*), two LFY targets regulated independently of *UFO*<sup>3,4,22</sup> that are required for organ identity of the first and second (*API*) or third and fourth (*AG*) floral whorls. We found that their activation by LFY and LFY–VP16 was insensitive to *UFO* (Fig. 1c,d). Thus, the protoplast assay accurately reproduced several floral promoter activation patterns.

We next investigated the involvement of an SCF<sup>UFO</sup>-dependent ubiquitination pathway in *pAP3* activation by LFY–UFO. We found that, when co-expressed with LFY, amino-terminally truncated *UFO* versions lacking the F-box domain (*UFOΔFbox* and *UFOΔFbox*–VP16) activated *pAP3* similarly to the full-length (FL) *UFO* (Fig. 1e). The connection of *UFO* to an SCF complex thus appears dispensable for *pAP3* activation in transient protoplast assays. The previously reported inactivity of *UFO* with an internal deletion of its F-box probably reflects the poor folding of this protein variant rather than the functional importance of the F-box domain (Extended Data Fig. 1a–c)<sup>20</sup>.

We also constitutively expressed tagged versions of *UFO* and *UFOΔFbox* in *Arabidopsis*. Irrespective of the presence of the F-box, plants displaying a detectable *UFO* or *UFOΔFbox* expression (Extended Data Fig. 1d) showed a typical *UFO* gain-of-function phenotype (Fig. 1f,g). In addition, both *UFO* versions complemented the strong *ufo-1* mutant and induced gain-of-function phenotypes (Fig. 1h and Extended Data Fig. 1e,f)<sup>8</sup>. Still, minor defects (such as some missing or misshapen petals and disorganized flowers) were specifically observed in the absence of the F-box, suggesting that this conserved domain might be important for a subset of *UFO* functions (Fig. 1h and Extended Data Fig. 1g). Overall, *UFO* and *UFOΔFbox* have very similar activities, showing that the role of the F-box domain is largely dispensable

and that a ubiquitination-independent mechanism determines the LFY–UFO synergy.

## LFY and *UFO* form a transcriptional complex on a new DNA motif

Protoplast assays established that the *AP3* and *RBE* promoter sequences contain the information that dictates their specific activation by LFY–UFO. Several regulatory regions driving *AP3* regulation in early floral meristem have been identified, including the distal and proximal early elements (DEE and PEE; Fig. 2a)<sup>23,24</sup>. The DEE contains a predicted canonical LFYBS, but in protoplasts, like in plants<sup>24</sup>, this site is not sufficient to explain *pAP3* activation (Extended Data Fig. 2). By systematically testing *AP3* promoter variants in the transient assay, we identified a 20-base-pair (bp) DNA element around the PEE important for LFY–UFO-dependent activation but devoid of canonical LFYBS (Fig. 2b and Extended Data Fig. 3a–c). We investigated the possibility that LFY and *UFO* form a complex on this DNA element using electrophoretic mobility shift assays (EMSA). For this, we mixed either recombinant LFY–DBD (the LFY domain interacting with *UFO*)<sup>18</sup> or in-vitro-produced FL LFY with a reconstituted ASK1–*UFO* complex. None of the proteins bound the DNA probe alone, but a shift was observed when LFY–DBD or FL LFY was mixed with ASK1–*UFO* (Fig. 2c). Thus, a presumptive ASK1–*UFO*–LFY complex was formed on a *pAP3* DNA element (hereafter named LFY–*UFO* Binding Site 0 (LUBSO)) that each partner did not bind on its own. We did note that *UFO* had a weak affinity for DNA, as ASK1–*UFO* shifted the DNA probe when we performed EMSAs with low competitor DNA concentrations (Extended Data Fig. 3d). EMSAs performed with LUBSO mutated at various bases provided evidence that the formation of the complex is sequence-specific and suggests a bipartite DNA motif (Extended Data Fig. 3f).

To identify all genome regions possibly targeted by the ASK1–*UFO*–LFY complex, we performed amplified DNA affinity purification sequencing (ampDAP-seq) with a reconstituted ASK1–*UFO*–LFY complex (Extended Data Fig. 4a,b). We identified numerous genomic regions where LFY binding was strongly enhanced by the presence of ASK1–*UFO*. For each bound region, we computed the ratio (the coverage fold change (CFC)) between the coverage of peaks in the presence or absence of ASK1–*UFO* (Fig. 2d). Searches for enriched DNA motifs in the 600 regions with the highest CFC (>4.7) identified two bipartite motifs made of a 6-bp RRRRCA (N indicates A/C/G/T; R indicates A/G) sequence, four bases of variable sequence and either a monomeric or a dimeric site resembling canonical LFYBS but with more variability (Fig. 2e). Consistent with the presence of a sequence resembling LFYBS, we found that *pAP3* activation in protoplasts required the LFY amino acid residues involved in binding to canonical LFYBS (Extended Data Fig. 4c,d).

We named the identified motifs mLUBS and dLUBS for monomeric and dimeric LFY–*UFO* Binding Sites, respectively (Fig. 2e). Since it is observed specifically with ASK1–*UFO*, the RRRRCA element was named the *UFO* Recruiting Motif (URM). Position weight matrices (PWMs) for dLUBS and to a lesser extent mLUBS outperformed the canonical PWM for LFY, showing that they reliably predicted the binding of ASK1–*UFO*–LFY (Extended Data Fig. 4e). The LFYBS present within the LUBS of high-CFC regions tended to have a lower predicted affinity than those present in regions bound by LFY alone (Extended Data Fig. 4f), explaining why LFY binding to those sequences occurs only with *UFO* and the URM. Remarkably, we also identified the URM de novo from published LFY chromatin immunoprecipitation sequencing (ChIP-seq) data (Extended Data Fig. 4g)<sup>25</sup>. Moreover, we found that the LFY ChIP-seq performed in inflorescences<sup>25</sup> correlates better with the ASK1–*UFO*–LFY ampDAP-seq than with the LFY ampDAP-seq (Spearman rank correlation of 0.481 versus 0.338 for the first 1,000 ChIP-seq peaks), strongly suggesting that many regions are bound *in vivo* by *UFO* (see examples of such regions in Extended Data Fig. 7b,c).

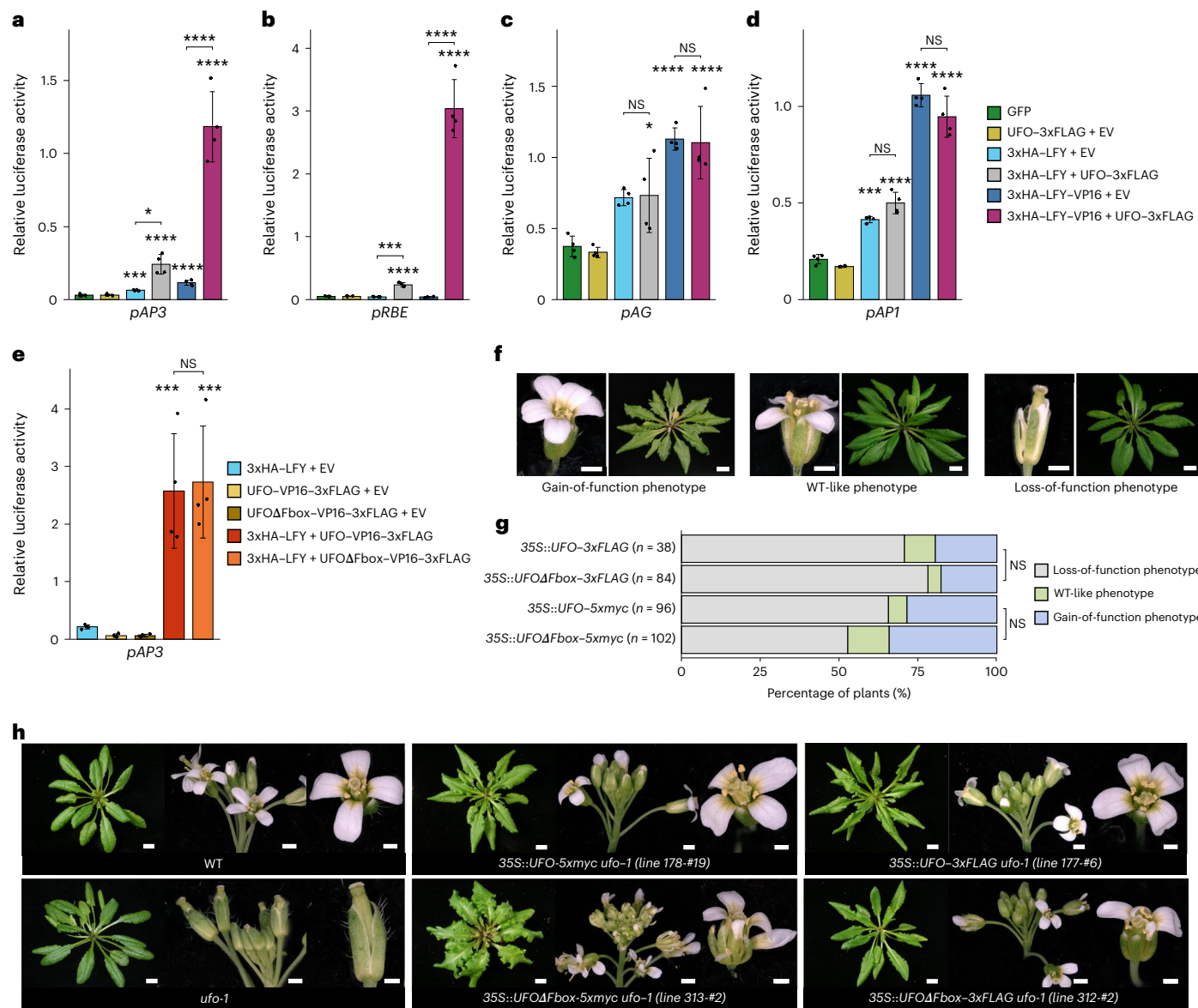


**Fig. 1 | UFO action is largely independent of its F-box domain.** **a–e**, Promoter activation in *Arabidopsis* protoplasts, with the indicated effectors (right) and promoters (below each graph). EV, empty vector. The data are mean  $\pm$  s.d. ( $n = 4$  biological replicates). We used one-way analysis of variance (ANOVA) with Tukey's multiple comparisons test (**a–e**) or Welch's ANOVA with Games–Howell post hoc tests (**b**). For **a** and **b**, the ANOVAs were performed on log-transformed data (Methods). The asterisks represent a significant statistical difference compared with GFP (**a–d**) or 3xHA-LFY + EV (**e**), non-significant (NS) otherwise. Other comparisons are indicated with brackets. NS,  $P > 0.05$ ; \* $P < 0.05$ ; \*\* $P < 0.001$ .

\*\*\* $P < 0.0001$ . **f**, Representative pictures of the different phenotypic classes obtained in the  $T_1$  population of the indicated transgenic plants (scale bars, 1 mm for flowers and 1 cm for rosettes). **g**, Distribution of  $T_1$  plants in phenotypic classes as described in **f**. The distribution of 35S::UFO and 35S::UFO $\Delta$ Fbox lines within phenotypic classes is not significantly different ( $\chi^2$  tests; NS,  $P > 0.05$ ).  $n$ , number of independent lines. **h**, *ufo-1* complementation assay by the 35S::UFO and 35S::UFO $\Delta$ Fbox transgenes. Rosettes (scale bars, 1 cm), inflorescences (scale bars, 1 mm) and flowers (scale bars, 0.5 mm) are shown. Source data are available in Supplementary Data 4.

The ampDAP-seq findings were validated by EMSAs with DNA probes corresponding to optimal mLUBS and dLUBS motifs (Fig. 2f and Extended Data Fig. 4h). We observed a complex of slower mobility with dLUBS than with mLUBS, consistent with the presence of two LFY molecules on dLUBS. ASK1–UFO also supershifted LFY bound to canonical LFYBS from *pAP1* and *pAP3* DEE (Extended Data Fig. 4i), sometimes (but not systematically) increasing apparent LFY binding.

## LUBS are functional regulatory elements

Examination of the *pAP3* genomic region in ASK1–UFO–LFY ampDAP-seq revealed a peak that is absent in the experiment performed with LFY alone (Fig. 3a). This peak is roughly located on the PEE and is

consistent with LFY ChIP-seq peaks<sup>25,26</sup>. We searched for LUBS under this peak, and, to our surprise, we identified several sites predicted to be better than LUBSO (Fig. 3a). In EMSAs, the two highest-scoring sites, LUBS1 and LUBS2, were specifically bound by LFY in the presence of ASK1–UFO (Fig. 3b and Extended Data Fig. 5a). EMSAs performed with a LFY mutant version affected in its ability to dimerize further confirmed the stoichiometry of LFY–UFO complexes on LUBS1 and LUBS2 (Extended Data Fig. 5b). A similar binding was also observed when combining LFY and UFO $\Delta$ Fbox (Extended Data Fig. 5c,d), consistent with the F-box being facultative for LFY–UFO transcriptional activity (Fig. 1). In the protoplast assay, altering LUBS1 or LUBS2 (or both) significantly reduced *pAP3* activation (Fig. 3c); the LUBS1 alteration had a stronger

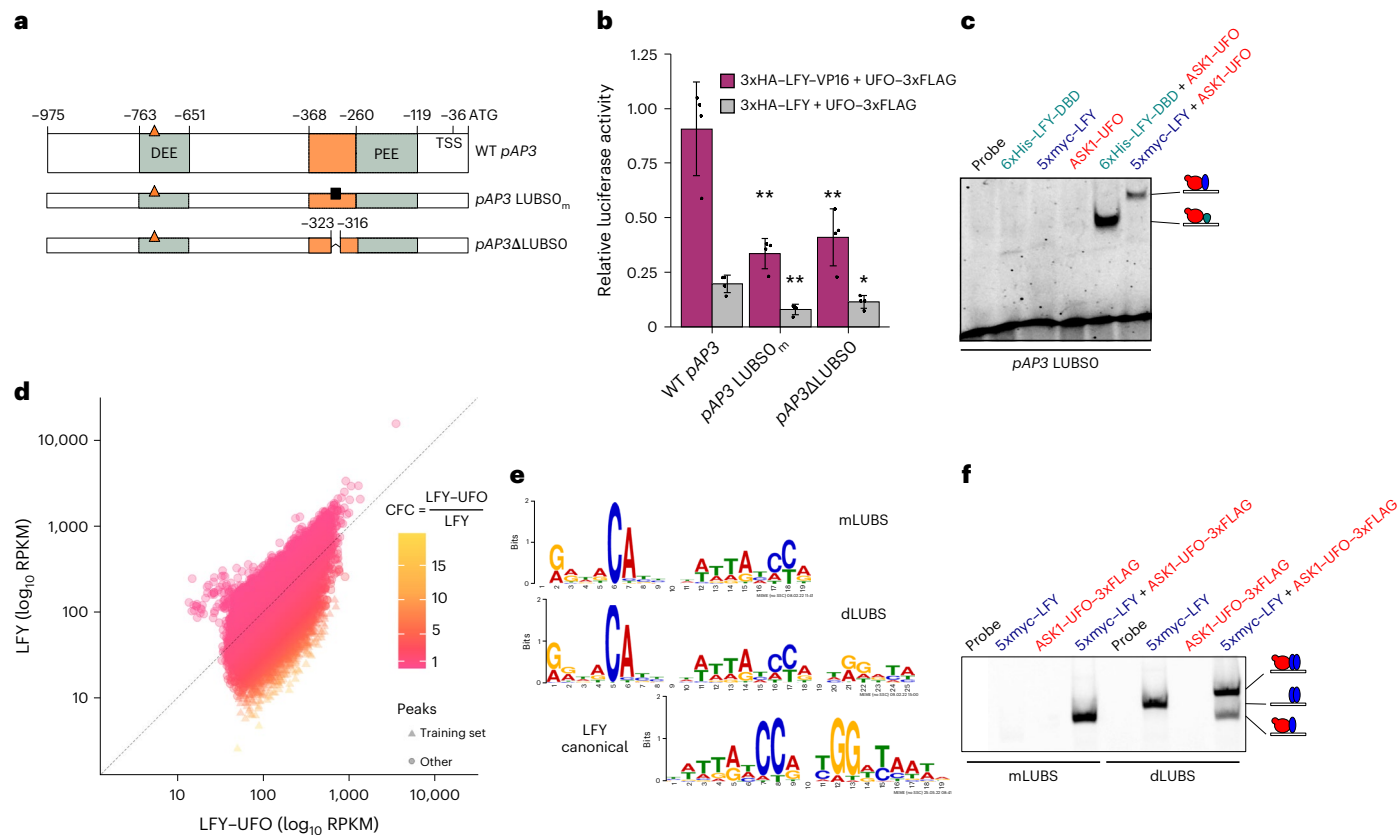


**Fig. 2 | LFY and UFO together bind a new DNA motif.** **a**, WT *pAP3* with regulatory regions and *cis*-elements (top line). The coordinates are relative to the *AP3* start codon. TSS, transcription start site. The orange triangles represent canonical LFYBS. The orange rectangle represents the 107-bp region and the black square represents the mutation introduced in *pAP3 LUBSO* (*LUBSO<sub>m</sub>*). The detailed functional dissection of the 107-bp region and the *LUBSO* mutation (*LUBSO<sub>m</sub>*) are described in Extended Data Fig. 3. The other rows show the promoter versions used in **b**. **b**, *pAP3* activation in *Arabidopsis* protoplasts. The data are mean  $\pm$  s.d. ( $n = 4$  biological replicates). We used one-way ANOVA with data from the same effector and Tukey's multiple comparisons tests. The asterisks represent a significant statistical difference compared with WT *pAP3* (\* $P < 0.05$ ; \*\* $P < 0.01$ ). **c**, EMSA with *LUBSO* DNA probe and the indicated proteins. Size exclusion chromatography (SEC) coupled to multi-angle laser light scattering

(MALLS) established a mass of  $102 \pm 3.3$  kDa for the ASK1-UFO-LFY-DBD-LUBSO complex, consistent with a 1:1:1:1 stoichiometry (Extended Data Fig. 3e). The drawings represent the different complexes with FL LFY (blue), LFY-DBD (pale blue) and ASK1-UFO (red) on DNA. **d**, Comparison of peak coverage in LFY and LFY-UFO ampDAP-seq experiments, coloured by CFC. The LFY-UFO-specific peaks used to build the mLUBS and dLUBS motifs in **e** are triangle-shaped. RPKM, reads per kilobase per million. **e**, Logos for mLUBS, dLUBS and LFYBS. The LFY logo was generated using the 600 peaks with the strongest LFY ampDAP-seq signal. **f**, EMSAs with the mLUBS and dLUBS DNA probes that had the highest-scoring sequences. The drawings represent the different complexes with LFY (blue) and ASK1-UFO (red) on DNA. Source data are available in Supplementary Data 4.

effect. Specifically altering the URM of *pAP3 LUBS1* and *LUBS2*, which abolished LFY-UFO binding on individual sites in EMSAs (Extended Data Fig. 5e), also reduced *pAP3* activation, albeit less effectively than altering the whole LUBS (Extended Data Fig. 5f). Finally, the previously described *pAP3::GUS* staining pattern in the second and third whorls of early floral meristems in *Arabidopsis* was severely reduced when *LUBS1* and *LUBS2* were altered, demonstrating the importance of these sites *in vivo* (Fig. 3d and Extended Data Fig. 5g). Similarly, the *RBE* promoter contains an ASK1-UFO-LFY ampDAP-seq peak that is absent with LFY alone (Extended Data Fig. 6a), and the functional importance of the single LUBS identified under this peak was confirmed using EMSAs, transient assays in protoplasts and stable reporter constructs in plants (Extended Data Fig. 6b–e).

In addition to *AP3* and *RBE*, LFY and UFO together probably regulate many other genes in *Arabidopsis*. To identify such potential LFY-UFO targets, we established a list of genes bound (in ampDAP and ChIP) and regulated by LFY-UFO (Extended Data Fig. 7a). This procedure identified the other B gene *PISTILLATA* (*PI*), previously proposed as a LFY-UFO target but through an unknown regulatory element that the LUBS model precisely localized (Extended Data Fig. 7b). We also found floral regulators such as *SQUAMOSA PROMOTER BINDING PROTEIN*

*LIKE 5* and *FD* as well as additional candidates probably regulated by LFY and UFO (Extended Data Fig. 7a,c).

### The LFY K249R substitution specifically affects UFO-dependent LFY functions

In *Arabidopsis*, LFY performs UFO-dependent and independent functions<sup>3</sup>, and we wondered whether they could be uncoupled by introducing specific alterations in LFY. As we were initially looking for LFY ubiquitination mutants, we substituted exposed lysines of LFY-DBD with arginines and tested the effect of such alterations on LFY-UFO-dependent *pAP3* activation in protoplasts. We found one substitution (LFY K249R; Extended Data Fig. 8a) that strongly reduced *pAP3* activation by LFY-UFO (Fig. 4a) or LFY-VP16-UFO (Extended Data Fig. 8b) without affecting the UFO-independent *pAG* activation (Extended Data Fig. 8c) or the LFY-UFO interaction (Extended Data Fig. 8d). AmpDAP-seq experiments showed that the LFY K249R substitution specifically impaired the binding of LFY-UFO but not that of LFY alone (Fig. 4b,c and Extended Data Fig. 8e–i), revealing that Lys249 plays a key role in LFY-UFO interaction with the LUBS DNA.

The importance of LFY Lys249 for UFO-dependent LFY functions was also confirmed using complementation assays of the *Arabidopsis*

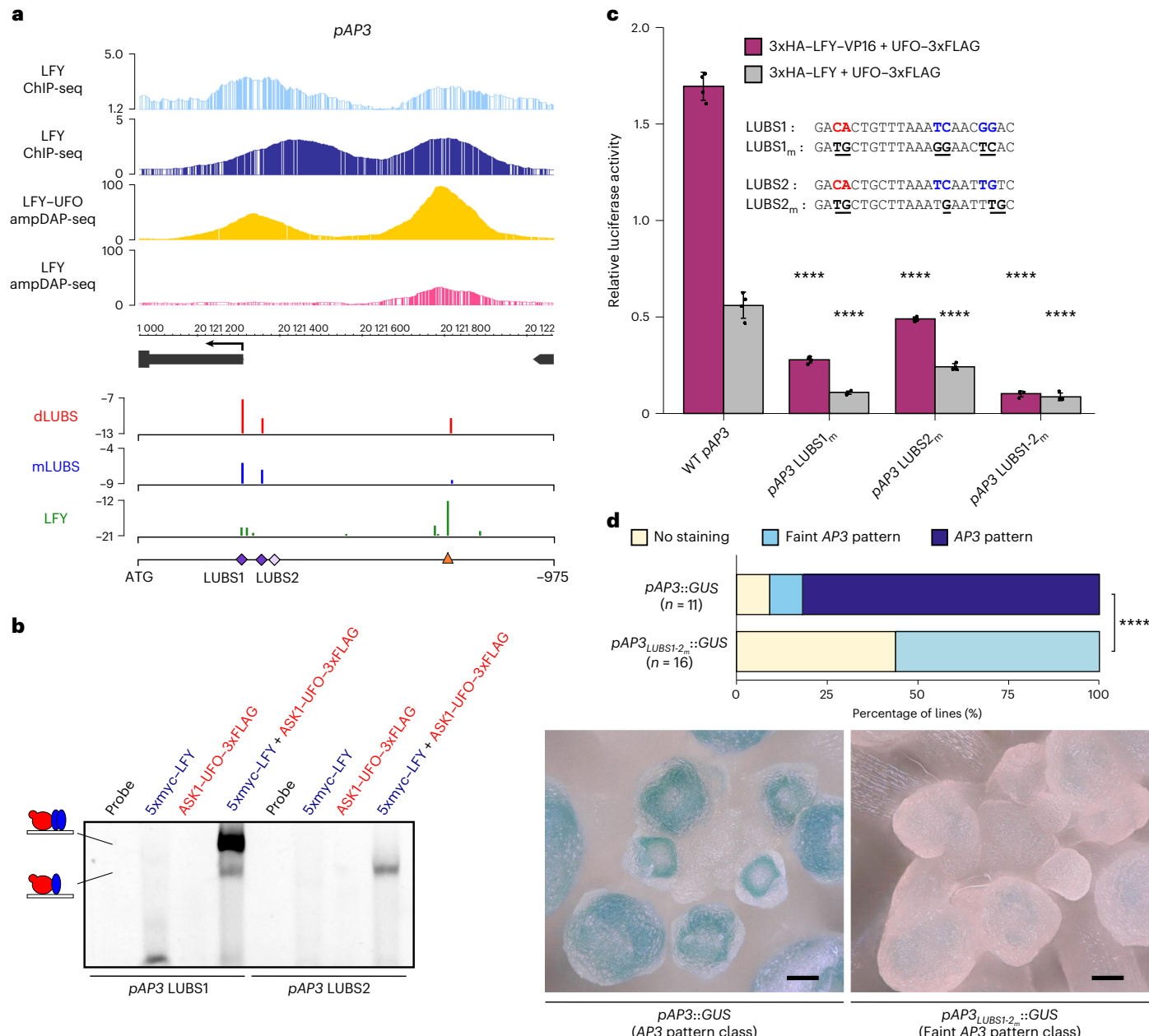


**Fig. 3 | Functional validation of LUBS.** **a**, Top, Integrated Genome Browser view of *pAP3* showing LFY ChIP-seq in inflorescences (light blue)<sup>25</sup> and seedlings (dark blue)<sup>26</sup>, LFY-UFO ampDAP-seq (yellow), and LFY ampDAP-seq (pink)<sup>48</sup>. The y axis indicates the read number range. Bottom, identification of LUBS in *pAP3*. The predicted binding sites using dLUBS and mLUBS models and the LFY PWM are shown; the y axis represents score values. LUBS1 and LUBS2 are indicated with purple diamonds, and canonical LFYBS is shown as an orange triangle. LUBS0 (light purple diamond) is not visible because of its low score. **b**, EMSAs with *pAP3* LUBS probes. The drawings represent the different complexes involving LFY (blue) and ASK1-UFO (red) on DNA. **c**, *pAP3* activation in *Arabidopsis* protoplasts. The effects of alterations (underlined) in URM (red) and LFYBS (blue) bases of *pAP3* LUBS were assayed. The data are mean  $\pm$  s.d. ( $n = 4$  biological replicates).

One-way ANOVAs were performed with data from the same effector (one-way ANOVA with Tukey's multiple comparisons tests for 3xHA-LFY + UFO-3xFLAG data and Welch's ANOVA with Games-Howell post hoc tests for 3xHA-LFY-VP16 + UFO-3xFLAG data). The asterisks represent a statistical difference compared with the WT promoter ( $^{****}P < 0.0001$ ). **d**, *In vivo* analysis of *pAP3::GUS* fusions. The percentage of transgenic lines with an AP3 pattern, a faint AP3 pattern or absence of staining is shown (top). The pattern distributions differ between the two constructs ( $\chi^2$  test;  $^{****}P < 0.0001$ ).  $n$ , number of independent lines. Representative pictures of plants with an AP3 pattern (bottom left) and a faint AP3 pattern (bottom right) are also shown. Scale bars, 50  $\mu$ m. Note the staining in the ring corresponding to the second and third whorl primordia in the left picture. Source data are available in Supplementary Data 4.

*Ify-12* null mutant<sup>27</sup>. *Ify-12* plants expressing LFY<sup>K249R</sup> or LFY<sup>K249S</sup> under the control of the *LFY* promoter developed flowers with normal sepals and carpels but with defective third-whorl and, more importantly, second-whorl organs, resulting in flowers similar to those observed in weak *ufo* mutants (Fig. 4d). When expressed under the constitutive 3SS promoter, LFY<sup>K249R</sup> triggered ectopic flower formation and early flowering like WT LFY (Extended Data Fig. 8j), consistent with these

LFY functions being independent of UFO and thus not affected by the K249R substitution<sup>28</sup>.

### Structural characterization of the ASK1-UFO-LFY-DNA complex

To understand how the LFY-UFO complex recognizes its cognate DNA binding site and how the Lys249 alteration impedes this interaction,

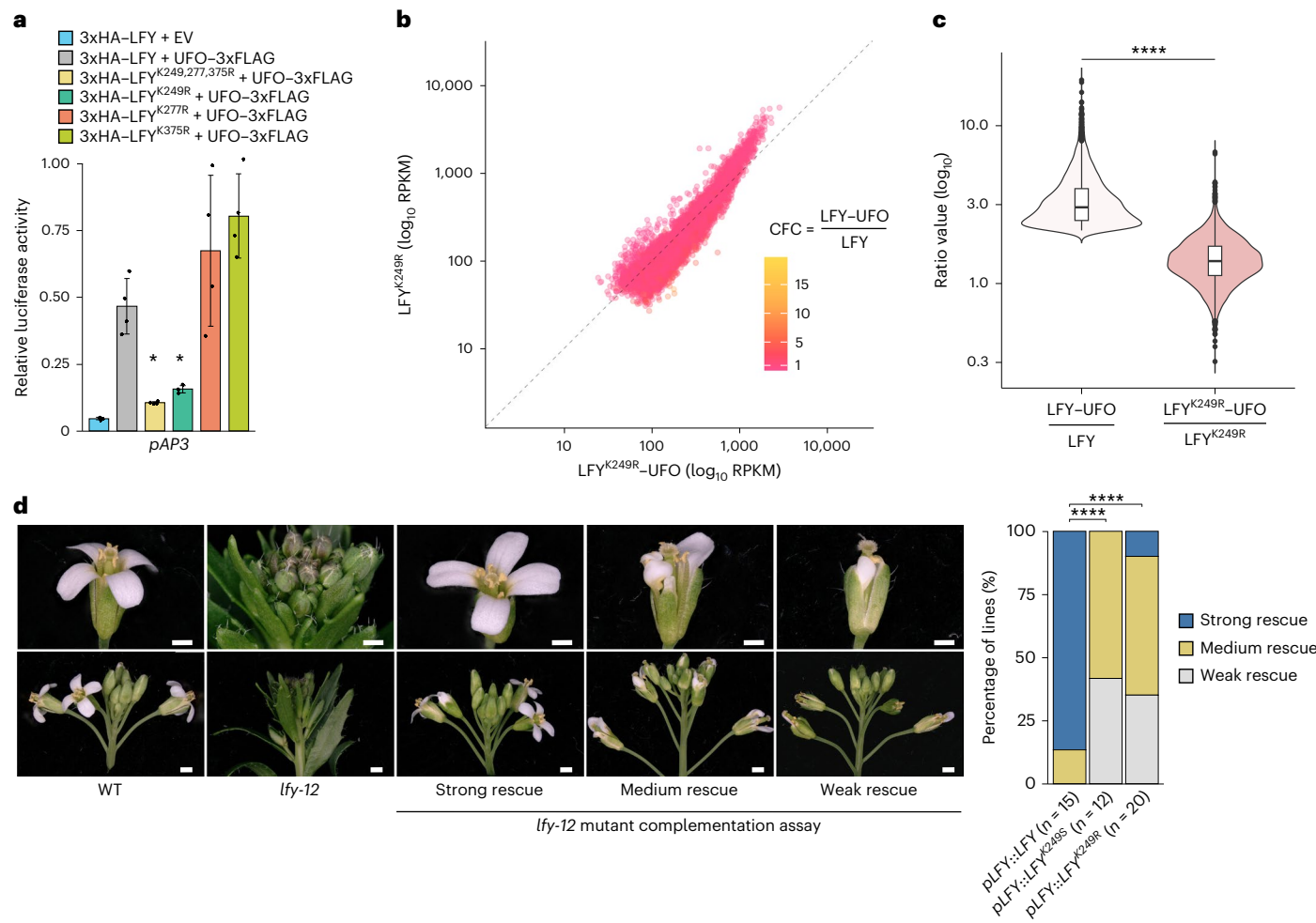


**Fig. 4 | The LFY K249R substitution disrupts the LFY–UFO synergy.** **a**, *pAP3* activation in *Arabidopsis* protoplasts. The data are mean  $\pm$  s.d. ( $n = 4$  biological replicates). We used Welch's ANOVA with Games–Howell post hoc tests. The asterisks indicate a statistical difference compared with 3xHA–LFY + UFO–3xFLAG (\* $P < 0.05$ ). **b**, Comparison of peak coverage in LFY<sup>K249R</sup>–UFO (xaxis) and LFY<sup>K249R</sup> (yaxis) ampDAP-seq experiments, coloured by peak CFC as in Fig. 2d. Note that, in contrast to Fig. 2d, the LFY–UFO-specific regions are mostly absent. **c**, Distribution of coverage ratios for LFY and LFY<sup>K249R</sup> for LFY–UFO-specific regions (20% highest CFC,  $n = 3,843$  genomic regions). We used a Wilcoxon rank sum test (\*\*P < 0.0001). The median (solid line), interquartile range

(box edges),  $\pm 1.5 \times$  the interquartile range (whiskers) and outliers (dots) are shown. **d**, *Ify-12* mutant complementation assay. The WT, the *Ify-12* mutant and representative plants of the different phenotypic complementation classes are shown on the left. Scale bars, 1 mm for the top row and 1 cm for the bottom row. The distribution of the different lines within the phenotypic complementation classes is shown on the right. Plants complemented with LFY<sup>K249R</sup> and LFY<sup>K249S</sup> show different complementation patterns than plants complemented with LFY ( $\chi^2$  tests; \*\*\*\*P < 0.0001).  $n$ , number of independent lines. Source data are available in Supplementary Data 4.

we purified the ASK1–UFO–LFY–DBD–LUBS1 complex and structurally characterized it using cryo-electron microscopy (cryo-EM) (Fig. 5a and Extended Data Fig. 9a–d). A structure at a 4.27 Å resolution was obtained (Extended Data Fig. 9g–i) into which were fit the AlphaFold2 predicted structures for UFO and ASK1, and the LFY–DBD dimer/DNA crystallographic structure<sup>29</sup> (PDB, 2VY1; Fig. 5b and Extended Data Fig. 9e,f). Due to the modest resolution, specific interacting amino acids could not be unambiguously identified. However, the major protein–protein and protein–DNA interaction surfaces were clearly identifiable.

The structure revealed that UFO directly contacts the DNA in the major groove around the URM (Fig. 5c). This binding probably involves basic residues present on loops projecting from the UFO Kelch-type β-propeller and results in a bend of roughly 30 degrees in the DNA double helix (Extended Data Fig. 9f). The structure also shows an interface between UFO and one LFY–DBD monomer (Fig. 5c). The LFY–DBD loop containing the Lys249 residue lies in this interface and probably interacts with one of the DNA-binding loops of UFO, consistent with the key role of LFY Lys249 in the ternary complex formation. As expected,

ASK1 interacts with the UFO F-box domain<sup>15</sup> (Fig. 5d). These data show how a β-propeller protein is able to modify the specificity of a TF, and they offer a structural explanation of how LFY and UFO synergistically recognize a specific DNA element via direct interactions by both proteins with the DNA.

## The LFY–UFO complex might have a deep evolutionary origin

As genetic and physical LFY–UFO interactions have been described in diverse angiosperms, we wondered whether the mechanism unravelled for *Arabidopsis* proteins could also apply to LFY from other species, including non-angiosperm ones. We selected LFY orthologous proteins from several species and with different DNA binding specificities (Fig. 6a). LFY specificity has evolved with three major DNA binding specificities<sup>30</sup>. Type I specificity is the one described in *Arabidopsis* and is valid for other angiosperms, gymnosperms, ferns and the moss *Marchantia polymorpha*, with two half-sites separated by a 3-bp spacer (Fig. 2e). LFY from the moss *Physcomitrium patens* has a type II

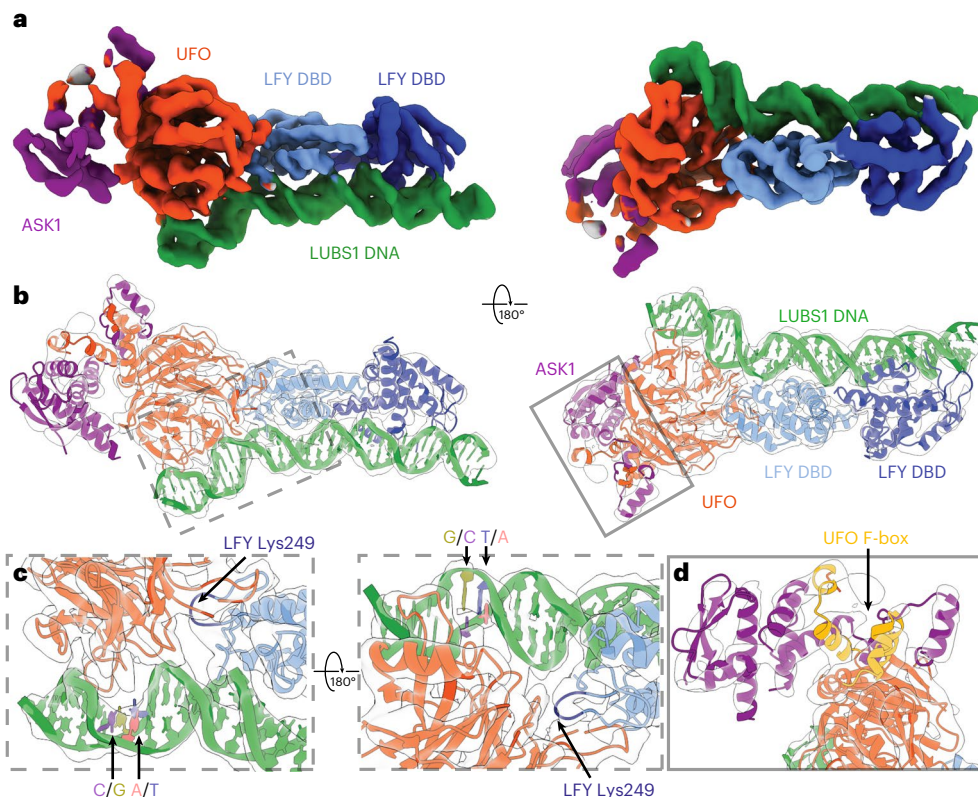


**Fig. 5 | Structural characterization of the ASK1–UFO–LFY–DNA complex.**

**a**, Cryo-EM density map of the ASK1–UFO–LFY–DBD–LUBS1 complex under two angles, coloured with regard to the underlying macromolecule (green for LUBS1 DNA, pale and dark blue for LFY–DBD, red for UFO, and purple for ASK1). **b**, The same views of the cryo-EM density map in transparent grey with fitted structures of the LFY–DBD dimer, UFO, ASK1 and LUBS1 DNA. The colours are the same as in **a**. The frames roughly indicate the regions shown in **c** and **d**. **c**, Zoom on the

UFO–DNA contact region (left) and on the LFY–UFO interface (right). Only the high-information CA of the URM and its complement are highlighted by filled colouring the rings for each base (red for A, blue for T, pale green for G and purple for C). The LFY–DBD loop containing the Lys249 residue is highlighted in dark blue. **d**, Zoom on the ASK1–UFO interface, with the UFO F-box highlighted in gold. Source data are available in Supplementary Data 4.

specificity with specific half-sites (different from type I half-sites) also separated by a 3-bp spacer. Finally, type III specificity is found for LFY from algae and corresponds to a type II motif without the spacer. Because functional UFO homologues have not been identified outside angiosperms, we used *Arabidopsis* UFO (AtUFO) in all the following experiments.

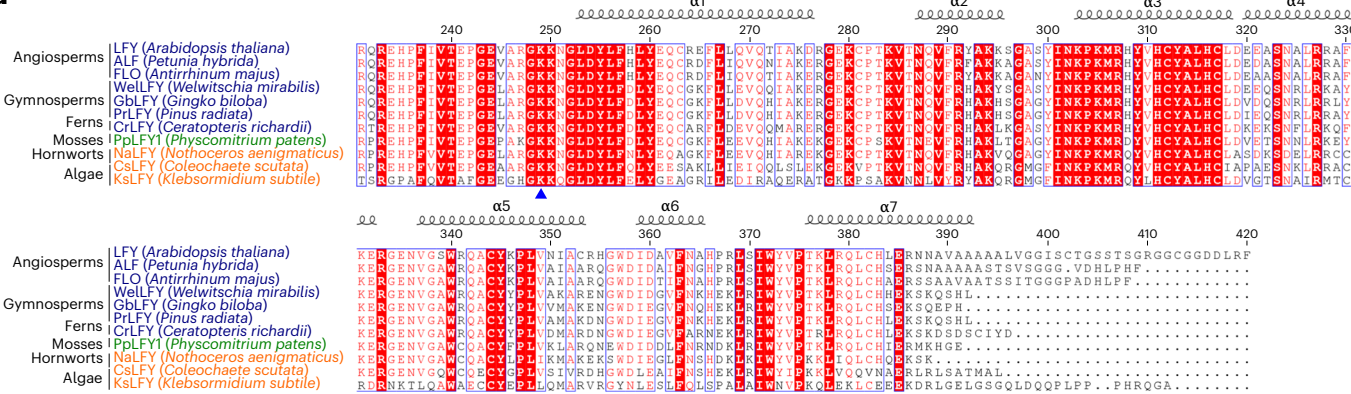
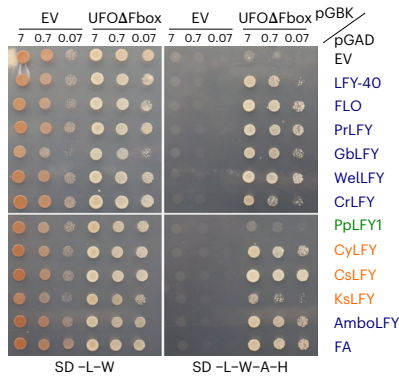
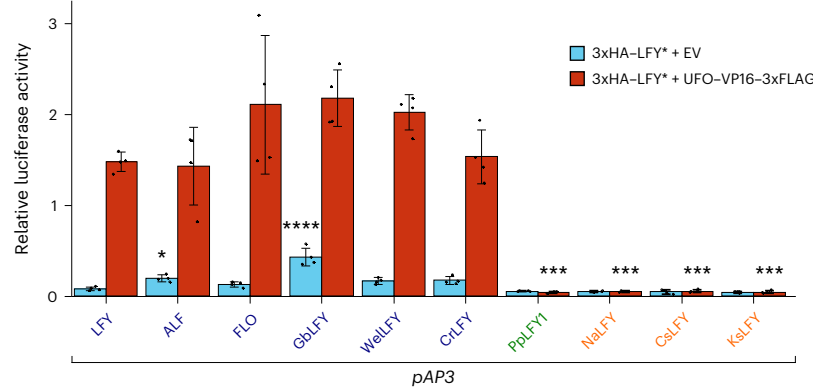
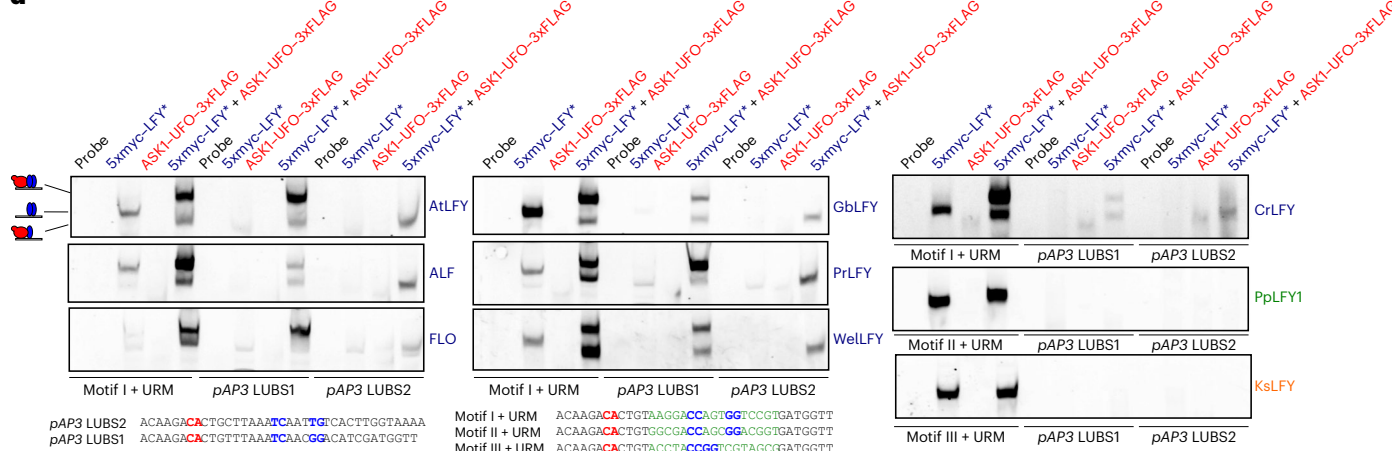
We tested the interactions of various LFY orthologues with AtUFO in yeast two-hybrid (Y2H) (Fig. 6b), in DLRA in protoplasts with *Arabidopsis* pAP3 (Fig. 6c) and in EMSAs (Fig. 6d). In Y2H, all LFYs except LFY from *P. patens* (type II) interacted with AtUFO (Fig. 6b). However, only type I LFYs from angiosperms, gymnosperms and ferns formed a complex on pAP3 LUBS and activated pAP3 in the protoplast assay (Fig. 6c,d). These results suggest that the ability of LFY and UFO to act together by forming a complex is ancient, largely predating the origin of angiosperms. We obtained no evidence that type II and III LFYs (from moss and algae) could form a complex with AtUFO on LUBS1 and LUBS2. A detailed and more trustworthy history of the LFY–UFO interaction will await further analyses, notably with the identification of UFO orthologues from non-angiosperm genomes.

## Discussion

LFY has long been known to interact with UFO to control flower and inflorescence development in numerous angiosperm species. However, the molecular nature of their synergistic action remained unknown. As UFO encodes an F-box protein taking part in an SCF complex<sup>17,31,32</sup>, it was thought to target proteins for SCF<sup>UFO</sup>-dependent ubiquitination

and possible degradation. LFY was an obvious target candidate, but clear evidence of LFY ubiquitination was missing<sup>12,18</sup>. The results we present here suggest that the F-box domain, required for ubiquitination, is dispensable for most UFO-dependent LFY activity. Nevertheless, the high conservation level of the UFO F-box sequence in angiosperms, together with slight differences in UFO activity when the F-box is deleted, suggests that this domain might still be needed for some elusive facets of UFO function. UFO may work redundantly with other F-box proteins in ubiquitination pathways, such as the F-box protein HAWAIIAN SKIRT identified in a genetic screen as an enhancer of the *ufo* mutant phenotype<sup>33</sup>. It is thus possible that UFO acts as a moonlighting protein<sup>34</sup> with functions in both transcription and ubiquitination, and these two activities could be related or independent.

The molecular mechanism we discovered here is consistent with most published data on AP3 and PI regulation<sup>18,23,35,36</sup>. However, a detailed understanding of the expression patterns of AP3 and RBE will require further work on other *cis*- and *trans*-elements. Why AP3 is not transcribed in floral stage 0–1 despite the expression of LFY and UFO is unclear<sup>20</sup>. It could be because SUPPRESSOR OF OVEREXPRESSION OF CO 1 (SOC1), AGAMOUS-LIKE 24 (AGL24) and SHORT VEGETATIVE PHASE (SVP) act as early AP3 repressors, as AP3 mRNA is detected in the floral anlage in a *soc1 svp agl24* mutant<sup>37,38</sup>. Another explanation could be that AP3 expression requires the SEPALLATA3 activator<sup>39</sup>. Why pAP3 is not activated by LFY (or LFY–VP16) alone through the canonical LFYBS is also an open question.

**a****b****c****d****Fig. 6 | LFY-UFO interaction is conserved beyond angiosperm species.**

**a**, Alignment of LFY DBDs. The amino acid numbering and secondary structure annotation are based on LFY from *A. thaliana*. The LFY Lys249 residue is indicated with a blue triangle. DNA binding specificities are colour-coded: types I (blue), II (green) and III (orange). FLO, FLORICAULA; ALF, ABERRANT LEAF AND FLOWER. **b**, Interaction between LFY orthologues and AtUFO $\Delta$ Fbox in Y2H. The LFY orthologues are described in **a** except CyLFY (*Cylindrocystis* sp.), AmboLFY (*Amborella trichopoda*) and FA (*FALSIFLORA; Solanum lycopersicum*). SD, synthetic defined. See Extended Data Fig. 4d for the legends. **c**, pAP3 activation measured by DLRA in *Arabidopsis* protoplasts. 3xHA-LFY\* refers to the different LFY orthologues indicated under the x axis. The data represent averages of independent biological replicates and are presented as mean  $\pm$  s.d., with each dot

representing one biological replicate ( $n = 4$ ). One-way ANOVAs were performed with data from the same effector (one-way ANOVA with Tukey's multiple comparisons tests for 3xHA-LFY\* + EV data and Welch's ANOVA with Games-Howell post hoc tests for 3xHA-LFY\* + UFO-VP16-3xFLAG data). The asterisks represent a statistical difference compared with AtLFY (\* $P < 0.05$ ; \*\* $P < 0.001$ ; \*\*\* $P < 0.0001$ ). **d**, EMSAs with the indicated DNA probes (bottom). URM and LFYBS bases are depicted in red and blue, respectively. The pAP3 LUBS1 sequence was modified to insert the perfect sequence of motif I, II or III<sup>30</sup> (depicted in green); these DNA probes were used as positive controls for the binding of LFYs alone and for LFY-UFO complex formation. 5xmyc-LFY\* refers to the different LFY orthologues indicated next to each EMSA and described in **a**. Source data are available in Supplementary Data 4.

Our work unravelled an unsuspected function unrelated to ubiquitination for UFO: it forms a transcriptional complex with LFY at regulatory sites that are different from the canonical sites bound by a LFY homodimer. UFO was previously proposed to act in transcription,

but in the absence of direct evidence that a LFY-UFO complex forms on new binding sites, it was difficult to understand how UFO controls only a subset of LFY targets. These new regulatory sites (mLUBS and dLUBS) are made of a low-affinity or half LFYBS (poorly or not bound

by LFY alone) and a motif located at a fixed distance from it and responsible for UFO recruitment. The formation of such a sequence-specific complex is explained at the structural level by the capacity of UFO to interact with both LFY and DNA. The poor ability of UFO to bind DNA alone explains its complete dependence on LFY to perform its transcriptional functions in planta<sup>6,20</sup>. Thus, depending on the *cis*-elements present in regulatory regions, LFY either binds DNA as a homodimer or requires UFO to form a ternary complex. The alteration of the LFY Lys249 residue allows these two types of binding to be uncoupled by specifically disrupting the formation of the LFY–UFO–DNA complex. The position of this residue in the three-dimensional structure at the interface among LFY, UFO and DNA is consistent with the key role of this residue in the complex formation. It is possible that replacing Lys249 with a bulkier Arg residue displaces the UFO loops involved in DNA binding without affecting the LFY–UFO interaction. Obtaining a higher-resolution structure will help us precisely understand the interactions occurring in this complex.

Although it might be a common regulatory mechanism, only a few cases where non-TF proteins modify TF DNA binding specificity have been described so far (for example, Met4 and Met28 modifying the binding of TF Cbf1 in yeast<sup>40</sup>, or the herpes simplex virus transcriptional activator VP16 changing the specificity of the Oct-1/HCF-1 complex<sup>41</sup>). None of these examples involves an F-box protein or a Kelch-type  $\beta$ -propeller protein, and none has been characterized at the structural level. The modification of TF DNA binding specificity by non-TF proteins offers additional possibilities for the combinatorial control of gene expression and explains how a master regulator such as LFY accesses specific *cis*-elements to perform different functions in distinct territories.

Since LFY and UFO play key roles together in numerous plant species (including ornamental, crop and model plants), our findings expand the molecular understanding of flower and inflorescence development in a large variety of angiosperms. Because the LFY–UFO synergy is observed with LFY orthologues from gymnosperms and ferns as well, we speculate that this complex largely predated the origin of flowers and could have been co-opted for flower development from a yet-unknown ancestral role.

## Methods

### *Arabidopsis* growth

All mutants and transgenic lines are in the *A. thaliana* Columbia-0 (Col-0) accession. Seeds were sown on soil, stratified for three days at 4 °C and then grown at 22 °C under long-day conditions (16 h light). Transgenic plants were obtained with *Agrobacterium tumefaciens* C58C1 pMP90 using the floral dip method. Transformants were identified using GFP or Basta selection.

### *Arabidopsis* cell suspension culture

*Arabidopsis thaliana* (ecotype Col-0) cells in suspension cultures were grown under continuous light (90  $\mu$ mol of photons per m<sup>2</sup> per s) at 21 °C with shaking in Murashige and Skoog medium supplemented with 30 g l<sup>-1</sup> sucrose and 2 mg l<sup>-1</sup> 2,4-dichlorophenoxyacetic acid, pH 5.5. The suspension cells were subcultured every week with a fivefold dilution. Suspension cells at four or five days following subculture were used for protoplast preparation.

### Cloning

DNA fragments were amplified by PCR with Phusion high-fidelity polymerase (NEB). Plasmids were all obtained by Gibson Assembly with either PCR-amplified or restriction-enzyme-digested backbone vectors. We used the 420-amino-acid LFY version. For site-directed mutagenesis, primers containing the desired mutations were used for Gibson Assembly mutagenesis. Plasmids were obtained using DH5 $\alpha$  bacteria and were all verified by Sanger sequencing. A list of plasmids and cloning procedures is provided in Supplementary Data 1. The oligonucleotide sequences are listed in Supplementary Data 2.

## Y2H

The coding sequences were cloned in pGADT7-AD or pGBTK7 vectors (Clontech) by Gibson Assembly. Y187 and AH109 yeast strains (Clontech) were transformed with pGADT7-AD or pGBTK7 vectors and selected on plates lacking leucine (SD–L) or tryptophan (SD–W), respectively (MP Biomedicals). After mating, the yeasts were restreaked on plates lacking leucine and tryptophan (SD–L–W) for two days. The yeasts were then resuspended in sterile water, and OD<sub>600nm</sub> was adjusted to the indicated values for all constructions; two tenfold dilutions were performed, and 6  $\mu$ l drops were done on SD–L–W or SD–L–W–A–H (lacking leucine, tryptophan, histidine and adenine) plates. The yeasts were grown at 28 °C, and pictures were taken at the indicated times.

### DLRAs in *Arabidopsis* protoplasts

Effector plasmids with a 3xHA tag were obtained by cloning the indicated genes in the modified pRT104 vector containing a 3xHA N-terminal tag (pRT104–3xHA)<sup>42</sup>. The pRT104 empty plasmid was reengineered to insert a 3xFLAG C-terminal tag. For reporter plasmids, the indicated promoter fragments were cloned upstream of a firefly luciferase gene in pBB174 (ref.<sup>43</sup>). We used a 975-bp *pAP3* fragment and a 2-kilobase (kb) *pRBE* promoter fragment upstream of the ATG, known to induce a WT pattern in planta<sup>23,44</sup>. *pAG* corresponds to the AG second intron fused to a minimal 3SS promoter, known to induce a WT pattern in planta<sup>22</sup>. For *pAPI*, we used a 600-bp fragment upstream of the ATG. This version is sufficient to give a WT pattern in planta<sup>45</sup>, and the use of longer promoter versions induced a very high background noise in protoplasts. The pRLC reference plasmid contains a *Renilla* luciferase sequence under the control of the 3SS promoter. Plasmids were obtained in large amounts using a NucleoBond Xtra Maxi Plus kit (Macherey-Nagel). Protoplasts were prepared from *Arabidopsis* Col-0 cell suspension and transformed following the procedure described by Iwata et al.<sup>46</sup>. The cell walls were digested using Onozuka R-10 cellulase and macerozyme R-10 (Yakult Pharmaceutical). The digested cells were passed through two layers of Miracloth to remove debris, and the protoplast concentration was adjusted to 2–5  $\times$  10<sup>5</sup> cells per ml. The protoplasts were then PEG-mediated transformed using 10  $\mu$ g of the indicated effector and reporter plasmids and 2  $\mu$ g of the reference plasmid. After 17 h of incubation at room temperature, the protoplasts were lysed. Firefly (F-LUC) and *Renilla* luciferase (R-LUC) activities were measured using a Dual Luciferase Reporter Assay System (Promega) and a TECAN Spark 10 M 96-well plate reader. F-LUC/R-LUC luminescence ratios were calculated with background-corrected values. Four biological replicates were done for each plasmid combination.

### EMSA

The DNA probes used in EMAS are listed in Supplementary Data 2. Complementary oligonucleotides were annealed overnight in annealing buffer (10 mM Tris (pH 7.5), 150 mM NaCl and 1 mM EDTA). Then, 4 pmol of double-stranded DNA was fluorescently labelled with 1 unit of Klenow fragment polymerase (NEB) and 8 pmol of Cy5-dCTP (Cytiva) in Klenow buffer for 1 h at 37 °C. The enzymatic reaction was stopped with a 10 min incubation at 65 °C.

The proteins used in EMAS were obtained by different methods (bacteria, insect cells or quick coupled transcription/translation (TnT)). The concentrations of recombinant proteins (6xHis–LFY–DBD and UFO $\Delta$ Fbox–3xFLAG) and recombinant complexes (ASK1–UFO and ASK1–UFO–3xFLAG) were adjusted to 500 nM for all reactions. All the 5xmyc-tagged proteins were obtained in vitro by TnT. We did 50  $\mu$ l TnT reactions by mixing 5  $\mu$ g of pTNT–5xmyc plasmid containing the gene of interest with TnT SP6 High-Yield Wheat Germ Protein Expression System (Promega) for 2 h at 25 °C. For EMAS with TnT-produced proteins, 5  $\mu$ l of TnT reaction was used. Recombinant protein buffer or TnT mix was used as a control when comparing reactions with multiple proteins.

All binding reactions were performed in 20  $\mu$ l of binding buffer (20 mM Tris (pH 7.5), 150 mM NaCl, 1% glycerol, 0.25 mM EDTA, 2 mM

MgCl<sub>2</sub>, 0.01% Tween-20 and 3 mM TCEP) with 10 nM labelled probe. The reactions were supplemented with 140 ng µl<sup>-1</sup> fish sperm DNA (Sigma-Aldrich) for EMSAs performed with in-vitro-produced LFY and 200 ng µl<sup>-1</sup> for EMSAs performed with recombinant 6xHis–LFY–DBD. The binding reactions were incubated for 20 min on ice and then loaded on a 6% native polyacrylamide gel. The gels were electrophoresed at 90 V for 75 min at 4 °C and revealed with an Amersham ImageQuant 800 imager (Cytiva). The uncropped gels are shown in the Source data.

### Recombinant protein production and purification from bacteria

We produced 6xHis–LFY–DBD in *E. coli* Rosetta2 (DE3) cells (Novagen) and purified it as previously described<sup>29</sup>. ASK1 was cloned into the pETM-11 expression vector<sup>47</sup>, and the resulting plasmid was transformed into *E. coli* BL21 cells (Novagen). The bacteria were grown in LB medium supplemented with kanamycin and chloramphenicol at 37 °C up to an OD<sub>600nm</sub> of 0.6. The cells were then shifted to 18 °C, and 0.4 mM isopropyl β-D-1-thiogalactopyranoside was added. After an overnight incubation, the cells were sonicated in UFO buffer (25 mM Tris (pH 8), 150 mM NaCl and 1 mM TCEP) supplemented with one EDTA-free Pierce Protease Inhibitor Tablet (Thermo Fisher). The lysed cells were then centrifuged for 30 min at 27,000 g. The supernatant was mixed with Ni Sepharose High Performance resin (Cytiva) previously equilibrated with UFO buffer (25 mM Tris (pH 8), 150 mM NaCl and 1 mM TCEP). The resin was then washed with UFO buffer containing 20 and 40 mM imidazole. Bound proteins were eluted with UFO buffer containing 300 mM imidazole and dialysed overnight at 4 °C against UFO buffer without imidazole.

### Recombinant protein production and purification from insect cells

The different tagged versions of ASK1, LFY and UFO were cloned in acceptor and donor plasmids (pACEBac1, pIDK and pIDS, respectively; Geneva Biotech). The final acceptor plasmids containing the desired combination of coding sequences were obtained with Cre recombinase (NEB). DH10EmBacY-competent cells containing the baculovirus genomic DNA (bacmid) were transformed with the final acceptor plasmids. Blue-white selection was used to identify colonies with a recombinant bacmid with the acceptor plasmid inserted. Bacmid was then isolated from bacteria and mixed with X-tremeGENE HP DNA Transfection Reagent (Roche) to transfect Sf21 insect cells. At 96 h after transfection, supernatant containing the recombinant baculovirus (VO) was collected and used to infect fresh Sf21 cells. When the infected cells reached the day post arrest, V1 virus was collected. For large expression, Sf21 cells were infected with either V1 virus or frozen baculovirus-infected cells. The pellet of a 0.75 l culture was sonicated in 50 ml of UFO buffer supplemented with one EDTA-free Pierce Protease Inhibitor Tablet (Thermo Fisher). The sonicated cells were centrifuged for 1.5 h at 120,000 g at 4 °C. The supernatant was then incubated for 1 h at 4 °C with Ni Sepharose High Performance resin (Cytiva) previously equilibrated with UFO buffer. The beads were transferred into a column and washed with 20 column volumes of UFO buffer, then UFO buffer + 50 mM imidazole. Proteins were eluted with UFO buffer containing 300 mM imidazole. The elution was dialysed overnight at 4 °C against UFO buffer. TEV protease was added to cleave tags (0.01% w/w). When ASK1 was limiting compared with UFO, recombinant 6xHis–ASK1 from bacteria was added. The following day, the elution was repassed on Dextrin Sepharose High Performance (Cytiva) and Ni Sepharose High Performance resins (Cytiva) to remove tags and contaminants. For ASK1–UFO, ASK1–UFO–3xFLAG or UFOΔFbox–3xFLAG, the proteins were concentrated with a 30 kDa Amicon Ultra Centrifugal filter (Millipore) and further purified by SEC. For ASK1–UFO–LFY–DBD complex purification, contaminant DNA was removed by passing proteins on Q Sepharose High Performance resin (Cytiva) pre-equilibrated with UFO buffer. Increasing salt concentrations allowed us to obtain

DNA-free proteins. The indicated annealed HPLC-purified oligonucleotides (Supplementary Data 2) were then added and incubated with proteins on ice for 20 min. The proteins were concentrated with a 30 kDa Amicon Ultra Centrifugal filter (Millipore) and further purified by SEC.

### SEC and SEC–MALLS

SEC was performed with a Superdex 200 Increase 10/300 GL column (Cytiva) equilibrated with UFO buffer. Unaggregated proteins of interest were frozen in liquid nitrogen and stored at -80 °C. SEC–MALLS was performed with a Superdex 200 Increase 10/300 GL column (Cytiva) equilibrated with UFO buffer. For each run, 50 µl containing 1 mg ml<sup>-1</sup> of complex was injected. Separations were performed at room temperature with a flow rate of 0.5 ml min<sup>-1</sup>. The elutions were monitored by using a Dawn Heleos II for MALLS measurement (Wyatt Technology) and an Optilab T-rEX refractometer for refractive index measurements (Wyatt Technology). Molecular mass calculations were performed using ASTRA software with a refractive index increment (dn/dc) of 0.185 ml g<sup>-1</sup>.

### ampDAP-seq

We used pTnT–5xmyc–LFY<sup>48</sup> to produce 5xmyc–LFY in vitro using a TnT SP6 High-Yield Wheat Germ Protein Expression System (Promega). We used the ampDAP-seq libraries described in Lai et al.<sup>48</sup>. The ampDAP-seq experiments were performed in triplicates (LFY–UFO) or in duplicates (LFY<sup>K249R</sup> and LFY<sup>K249R</sup>–UFO).

A 50 µl TnT reaction producing 5xmyc–LFY was mixed with an excess of recombinant ASK1–UFO–3xFLAG (2 µg) and 20 µl of Pierce Anti-c-Myc Magnetic Beads (ThermoScientific). DAP buffer (20 mM Tris (pH 8), 150 mM NaCl, 1 mM TCEP and 0.005% NP40) was added to reach 200 µl. The mix was incubated for 1 h at 4 °C on a rotating wheel. The beads were then immobilized and washed three times with 100 µl of DAP buffer, moved to a new tube and washed once again. The ampDAP-seq input libraries (50 ng) were then added, and protein–DNA mixes were incubated for 1.5 h at 4 °C on a rotating wheel. The beads were immobilized and washed five times with 100 µl of DAP buffer, moved to a new tube and washed two more times. Finally, the beads were mixed with 30 µl of elution buffer (10 mM Tris (pH 8.5)) and heated for 10 min at 90 °C.

Immunoprecipitated DNA fragments contained in the elution were amplified by PCR according to the published protocol<sup>49</sup> with Illumina TruSeq primers. The remaining beads were mixed with 20 µl of 1× SDS–PAGE Protein Sample Buffer, and western blots were performed to check the presence of tagged proteins. The PCR products were purified using AMPure XP magnetic beads (Beckman Coulter) following the manufacturer's instructions. Library molar concentrations were determined by quantitative PCR using a NEBNext Library Quant Kit for Illumina (NEB). The libraries were then pooled with equal molarity. Sequencing was done on Illumina HiSeq (Genewiz) with the specification of paired-end sequencing of 150 cycles.

### GUS staining

The different promoter versions were cloned upstream of the *GUS* gene in the pRB14 backbone vector<sup>45</sup>. Transformants were selected with GFP seed fluorescence. The number of independent lines analysed for each construct is indicated in each figure. GUS staining was performed on the apex of primary inflorescences of *T.2* plants. Tissues were placed in ice-cold 90% acetone for 20 min at room temperature and then rinsed in GUS buffer without X-Gluc (0.2% Triton X-100, 50 mM NaPO<sub>4</sub> (pH 7.2), 2 mM potassium ferrocyanide and 2 mM potassium ferricyanide). The tissues were transferred to GUS buffer containing 2 mM X-Gluc substrate (X-Gluc DIRECT) and placed under vacuum for 5 min. The samples were then incubated overnight at 37 °C unless otherwise specified in the legend. Finally, the tissues were washed with different ethanol solutions (35%, 50% and 70%), and pictures were taken with a Keyence VHX-5000 microscope with a VH-Z100R objective.

## In planta overexpression and mutant complementation assays

Tagged versions of UFO and UFOΔFbox were cloned under the control of the 35S promoter in pEGAD<sup>50</sup>. Transformants were selected with Basta treatment. Overexpressing lines with a strong gain-of-function phenotype were crossed with the strong *ufo-1* mutant. Basta-resistant F<sub>2</sub> plants were individually genotyped to select *ufo-1*– homozygous plants. For this, a fragment was amplified by PCR with the oligonucleotides oGT1085 and oPR578 (Supplementary Data 2) and digested with DpnII enzyme (NEB). On the basis of the digestion profile, *ufo-1*– plants were kept and analysed once they reached flowering.

Altered versions of LFY were cloned in pETH29 (ref. <sup>29</sup>) or pCA26 (ref. <sup>51</sup>) to express LFY complementary DNA under the control of its endogenous promoter or the 35S promoter, respectively. For the *Ify-12* complementation assay, heterozygous *Ify-12*/+ plants were transformed. The transformants were selected with GFP fluorescence and genotyped with a previously described protocol<sup>45</sup> to select *Ify-12*– plants. The complementation assay was performed with T<sub>2</sub> plants and was based on the analysis of the first ten flowers from the primary inflorescence. Pictures were taken with a Keyence VHX-5000 microscope with a VH-Z20R objective.

## Western blots

For western blots on plant total protein extracts, the indicated tissues were crushed in 2× SDS-PAGE Protein Sample Buffer (100 mM Tris (pH 6.8), 20% glycerol, 2% SDS, 0.005% Bromophenol blue and 0.8% w/v dithiothreitol) at a 1:2 w/v ratio and boiled for 5 min. The samples were then loaded on a 12% acrylamide SDS-PAGE gel. For all western blots, transfer was performed with an iBlot2 Dry Blotting System (Invitrogen) using the default parameters. Membranes were blocked for 1 h at room temperature with 5% milk TBST and then incubated overnight at 4 °C with 5% milk TBST solution containing HRP-conjugated antibody (1:1,000 for anti-FLAG (Sigma-Aldrich; Cat. No. A8592) and 1:5,000 for anti-myc (Invitrogen; Cat. No. R951-25)). Revelation was performed with Clarity Western ECL substrate (Bio-Rad). Pictures were taken with a ChemiDoc MP Imaging System (BioRad). The uncropped gels are shown in the Source data.

## Cryo-EM sample preparation, data collection and data processing

An aliquot of the SEC-purified ASK1–UFO–LFY–LUBS1 complex was thawed on ice (see Supplementary Data 2 for the LUBS1 DNA sequence). Subsequently, 3.5 µl of the complex at 1 mg ml<sup>-1</sup> was deposited onto glow-discharged (25 mA, 30 s) C-flat Au grid R 1.2/1.3 300 mesh (Electron Microscopy Sciences), blotted for 5.5 s with force 0 at 20 °C and 100% humidity using a Mark IV Vitrobot (FEI, Thermo Fisher Scientific), and plunge-frozen in liquid ethane for specimen vitrification. A dataset of about 1,000 videos of 40 frames was acquired on a 200 kV Glacios (Thermo Fisher Scientific) electron microscope (Supplementary Data 3) at a nominal magnification of 36,000 with a physical pixel size of 1.145 Å.

The raw videos, acquired with SerialEM on a Gatan K2 Summit camera (Supplementary Data 3), were imported to Cryosparc live<sup>52</sup> for motion correction and CTF estimation. The dose-weighted micrographs were used for particle picking with crYOLO v.1.7.6 and the general model for low-pass filtered images<sup>53</sup>. Particle coordinates were imported to Cryosparc, where all subsequent steps were performed. After manual inspection, a subset of 761 micrographs was selected on the basis of CTF fit resolution, total and per-frame motion, average defocus and relative ice thickness. A raw particle stack of 282,567 images was extracted at a box size of 256 × 256 pixels<sup>2</sup>, binned twice and subjected to two-dimensional classification to remove false positive picks. A total of 207,392 particles from the selected class averages were re-extracted, re-centred at full size and submitted for a second round of two-dimensional classification. All class averages showing clear protein features were selected, and the resulting 147,849 particles were used

for ab initio reconstruction with three classes and subsequent heterogeneous refinement of the resulting volumes. Of those three classes, two looked like a protein–DNA complex, with the most apparent difference being the presence or absence of an extra electron density at one edge of the DNA helix. The last class had no recognizable features and was used as a decoy to remove ‘junk’ particles. Each subset and volume of the two first classes was refined separately with non-uniform refinement<sup>54</sup>, resulting in two distinct reconstructions of about 4.2 Å resolution, where the DNA model, the crystal structure of LFY–DBD and the AlphaFold2 models of UFO and ASK1 could be unambiguously fitted into the electron density. The second of these classes could fit a LFY–DBD dimer, while in the first class there was density only for the LFY–DBD molecule that directly interacts with UFO (Extended Data Fig. 9d). The unsharpened maps of each reconstruction were used for post-processing with DeepEMhancer<sup>55</sup>. The figures were prepared with Chimera<sup>56</sup> or ChimeraX<sup>57</sup>.

## Cryo-EM model building

Ideal B-form DNA was generated in Coot<sup>58</sup> and then manually built into the electron density. The resulting model was further refined using phenix.real\_space\_refine<sup>59</sup>. A single monomer of LFY–DBD was manually placed in the electron density, followed by fitting in ChimeraX<sup>57</sup>. The biological LFY–DBD dimer was then downloaded from the RCSB PDB (2VY)<sup>29</sup> and used as a guide to place the second LFY monomer, followed by fitting to density in ChimeraX. Alphafold models<sup>60</sup> of ASK1 (uniprot ID: Q39255) and UFO (uniprot ID: Q39090) were both downloaded from the EBI, preprocessed to remove low-confidence regions in phenix.process\_predicted\_model<sup>61</sup>, and then placed manually and fit to density in ChimeraX.

## Bioinformatic analyses

**Read mapping and peak calling.** Read processing and peak calling of LFY, LFY–UFO, LFY<sup>K249R</sup> and LFY<sup>K249R</sup>–UFO ampDAP-seq data were performed as previously published<sup>62</sup>. Briefly, the quality of sequencing data was analysed with fastQC v.0.11.7, and adapters were removed with NGmerge v.0.2\_dev<sup>63</sup>. Bowtie2 v.2.3.4.1 was used for mapping to the TAIR10 *A. thaliana* reference genome<sup>64</sup>. Reads mapped to a single location and with a maximum of two mismatches were retained. Duplicates were removed with the samtools dedup program v.1.8. Bound regions (that is, peaks) were identified with MACS2 v.2.2.7.1, using input DNA from Lai et al. as a control<sup>48</sup>. Consensus peaks were selected with MSPC v.4.0.0 (ref. <sup>65</sup>) by retaining peaks called in all replicates and resizing them by ±200 bp around the peak maximum for further analysis.

**Analyses of ampDAP-seq experiments.** To compare binding in different experiments, peaks were merged according to a previously published procedure<sup>62</sup>. Bound peaks were considered as common if they overlapped by at least 80%, while the remaining non-overlapping portion of either peak was <50%. Peaks that did not overlap by at least 50% were considered as new peaks. The same procedure was used to assess experimental reproducibility (comparisons between replicates of the same experiment), where peaks were normalized by the number of reads mapped in the library (RPKM).

As the fraction of reads mapped in peaks is much lower for LFY than LFY–UFO ampDAP-seq (~25% versus ~40%, respectively), normalizing the read count by all reads mapped along the genome would introduce a bias and estimate the LFY relative coverage (RPKM) towards lower values compared with LFY–UFO. In addition to this consideration, experimental proof from EMSAs suggests that UFO does not strongly affect the binding intensity of the complex at canonical LFYBS (which represent most peaks). Hence, the read count at each peak was normalized by the total number of reads mapped within all LFY and LFY–UFO merged peaks. Then, the mean normalized coverage from each experiment, divided by the peak size, was computed for each peak. The same strategy was applied when comparing LFY<sup>K249R</sup>

and LFY<sup>K249R</sup>-UFO (Fig. 4b), LFY<sup>K249R</sup> and LFY (Extended Data Fig. 8h), and LFY, LFY-UFO, LFY<sup>K249R</sup> and LFY<sup>K249R</sup>-UFO (Fig. 4c). The CFC was computed on merged peaks as the ratio between the mean normalized peak coverage in LFY-UFO and LFY (Fig. 2d) or the mean normalized coverage in LFY<sup>K249R</sup>-UFO and LFY<sup>K249R</sup> (Fig. 4b).

**Motif search in bound regions.** Merged peaks of the LFY and LFY-UFO datasets were sorted on the basis of decreasing CFC value. The top 600 peaks (that is, the highest CFC values) were used for a motif search using MEME-ChIP v.4.12.0 using the options nmeme, 600; meme-maxsize, 600\*1000; meme-nmotifs, 1; dreme-m, 0; and noecho and the JASPAR 2018 core plants non-redundant database<sup>66</sup>. For dLUBS, we used the options meme-minw, 20; meme-maxw, 30; while for mLUBS, we used meme-minw, 16; meme-maxw, 19. To retrieve the LFY motif in Fig. 2e, the 600 LFY ampDAP-seq peaks with the strongest coverage were fed to MEME-ChIP with the options nmeme, 600; meme-nmotifs, 1; meme-minw, 19; meme-maxw, 19; pal.

**Receiver operating characteristics analysis.** From the dataset of merged peak sets (peaks found in LFY or in LFY-UFO experiments or in both), the peaks were sorted on the basis of decreased CFC value, the top 20% peaks were selected, and among these, the first 600 used for motif determination were excluded to avoid overfitting, for a total of 3,243 final peaks. A negative set of the same size was created using a previously published method, which allows searching for sequences from the *A. thaliana* genome (TAIR10 reference) with the same GC content and genomic origin as the positive set<sup>67</sup>. Both sets were scanned with dLUBS and mLUBS PWMs as well as with the LFY PWM with dependencies as published previously<sup>68</sup> using an in-house script available on our GitHub page. The receiver operating characteristics plot was then created with the R package plotROC v.2.2.1 (ref. <sup>69</sup>).

**LFY in dLUBS within LFY-UFO-specific regions versus LFY in LFY-specific regions.** To assess whether the scores of LFYBS within dLUBS were comparable to the scores of canonical LFYBS, we used the peaks from the comparison of LFY versus LFY-UFO ampDAP-seq and resized them ( $\pm 50$  bp around the peak maximum). We used the dLUBS matrix to scan the resized sequences and retained the best site per sequence. We then retrieved sequences corresponding to the dLUBS site and computed the score of the LFYBS present in dLUBS using the LFY PWM<sup>68</sup>. The values obtained in the 20% most LFY-UFO-specific sequences (20% highest CFC) are shown in the box plot. The 20% lowest CFC peaks were scanned with the LFY PWM to generate the box plot in Extended Data Fig. 4f.

**Microarray data analysis.** Microarray data were retrieved from AtGenExpress<sup>70</sup> for inflorescence tissue in the *ufo* background (ATGE\_52A-C) versus the Col-0 background (ATGE\_29A-C). The R package gcrma<sup>71</sup> was used to adjust probe intensities and convert them to expression measures, and then the limma package<sup>72</sup> was used to fit the model and smooth standard errors. A Benjamini–Hochberg correction was applied to the *P* values, and fold change (FC) was computed as the ratio between expression in the WT and that in the *ufo* mutant. Only genes with  $|\log_2(\text{FC})| > 0.5$  and adjusted  $P < 0.05$  were considered as significantly differentially expressed.

**ChIP-seq datasets and analysis of ChIP-seq versus ampDAP-seq.** We collected the raw data of all available LFY ChIP-seq datasets: GSE141704 (ref. <sup>73</sup>), GSE96806 (ref. <sup>25</sup>), GSE64245 (ref. <sup>26</sup>) and GSE24568 (ref. <sup>68</sup>). Mapping and peak-calling analysis were performed with the same procedure as for ampDAP-seq, except that the peaks were resized to 600 bp around the peak maximum, and the q option of MACS2 was set to 0.1. Coverage of the resulting peaks was calculated as the average of the normalized read coverage for each replicate. Peaks from the four datasets were merged through a four-way comparison following the

same procedure used for ampDAP-seq. Bedtools intersect (v.2.30.0)<sup>74</sup> was used with the options wa; f, 0.8; F, 0.8; and e to find the peaks common to the merged ChIP-seq peaks and the 20% most LFY-UFO-specific genomic regions (the highest CFC value from ampDAP-seq). The peaks were assigned to genes by extending gene regions 3 kb upstream of the transcription start site and 1 kb downstream of the transcription termination site and using bedtools intersect (options f, 0.8; F, 0.8; e). The bound genes obtained were crossed with the list of differentially expressed genes in *ufo* inflorescences.

**Identification of the URM from published LFY ChIP-seq data.** To test whether the URM could be identified de novo (Extended Data Fig. 4g), we collected the 298 regions bound by LFY ChIP-seq data from inflorescence tissue<sup>25</sup> for which the binding intensity was twice greater in vivo relative to in vitro (LFY ampDAP-seq). We resized these regions to  $\pm 55$  bp around the ChIP-seq peak maximum. The corresponding sequences were searched with the LFY PWM<sup>68</sup> to identify all LFYBS with a PWM score greater than -23. Assuming that a recruiting motif should be at a fixed distance from the LFYBS, we created 140 batches, corresponding to sequences with sizes ranging from 4 to 10 bp, distant from 1 to 20 bp at both sides of the canonical LFYBS. Each of the 140 batches of sequences was used as input with MEME-ChIP for motif discovery with the motif size constrained to the length of the sequences in a given batch.

### Statistics and reproducibility

All DLRA data were analysed using RStudio software<sup>75</sup> and are presented as mean  $\pm$  s.d. All statistical methods are indicated in the figure legends. One-way ANOVA was used to analyse experimental data with more than two experimental groups (with two-sided Tukey's multiple comparisons tests). Welch's ANOVA was performed when the homogeneity-of-variance assumption was not met (with two-sided Games–Howell post hoc tests). For Fig. 1a,b, the strong promoter activation by 3xHA-LFY-VP16 + UFO-3xFLAG skewed the model and did not allow us to analyse other differences; a log-transformation was applied to the data before performing ANOVA. Two-tailed unpaired Student's *t*-tests were used for the other data analyses. For the GUS experiments and plant complementation assays, two-sided  $\chi^2$  tests were used to test for independency between constructs and measured phenotypes. The raw data and exact *P* values are provided in the Source data files as well as the number of independent repetitions for each experiment.

### Reporting summary

Further information on research design is available in the Nature Portfolio Reporting Summary linked to this article.

### Data availability

The ampDAP-seq data have been deposited at GEO and are publicly available as of the date of publication (GSE204793). The cryo-EM structure determined in this study is deposited in the EM data bank under the reference number EMD-15145. The .pdb file of the model is available in the Supplementary Information. Any additional information required to reanalyse the data reported in this paper is available from the corresponding author upon request. The biological materials generated in this study are available from the corresponding author without restriction. Source data are provided with this paper.

### Code availability

All original code has been deposited at GitHub ([https://github.com/Bioinfo-LPCV-RDF/LFYUFO\\_project](https://github.com/Bioinfo-LPCV-RDF/LFYUFO_project)) and is publicly available as of the date of publication.

### References

1. Moyroud, E., Kusters, E., Monniaux, M., Koes, R. & Parcy, F. LEAFY blossoms. *Trends Plant Sci.* **15**, 346–352 (2010).

2. Irish, V. F. The flowering of *Arabidopsis* flower development. *Plant J.* **61**, 1014–1028 (2010).
3. Parcy, F., Nilsson, O., Busch, M. A., Lee, I. & Weigel, D. A genetic framework for floral patterning. *Nature* **395**, 561–566 (1998).
4. Wagner, D., Sablowski, R. W. M. & Meyerowitz, E. M. Transcriptional activation of APETALA1 by LEAFY. *Science* **285**, 582–584 (1999).
5. Lohmann, J. U. et al. A molecular link between stem cell regulation and floral patterning in *Arabidopsis*. *Cell* **105**, 793–803 (2001).
6. Lee, I., Wolfe, D. S., Nilsson, O. & Weigel, D. A LEAFY co-regulator encoded by UNUSUAL FLORAL ORGANS. *Curr. Biol.* **7**, 95–104 (1997).
7. Levin, J. Z. & Meyerowitz, E. M. UFO: an *Arabidopsis* gene involved in both floral meristem and floral organ development. *Plant Cell* **7**, 529–548 (1995).
8. Wilkinson & Haughn UNUSUAL FLORAL ORGANS controls meristem identity and organ primordia fate in *Arabidopsis*. *Plant Cell* **7**, 1485–1499 (1995).
9. Krizek, B. A. & Meyerowitz, E. M. The *Arabidopsis* homeotic genes APETALA3 and PISTILLATA are sufficient to provide the B class organ identity function. *Development* **122**, 11–22 (1996).
10. Ikeda-Kawakatsu, K., Maekawa, M., Izawa, T., Itoh, J.-I. & Nagato, Y. ABERRANT PANICLE ORGANIZATION 2/RFL, the rice ortholog of *Arabidopsis* LEAFY, suppresses the transition from inflorescence meristem to floral meristem through interaction with APO1. *Plant J.* **69**, 168–180 (2012).
11. Lippman, Z. B. et al. The making of a compound inflorescence in tomato and related nightshades. *PLoS Biol.* **6**, e288 (2008).
12. Souer, E. et al. Patterning of inflorescences and flowers by the F-box protein DOUBLE TOP and the LEAFY homolog ABERRANT LEAF AND FLOWER of petunia. *Plant Cell Online* **20**, 2033–2048 (2008).
13. Kuzay, S. et al. WAPO-A1 is the causal gene of the 7AL QTL for spikelet number per spike in wheat. *PLoS Genet.* **18**, e1009747 (2022).
14. Ingram, G. C. et al. Dual role for fimbriata in regulating floral homeotic genes and cell division in *Antirrhinum*. *EMBO J.* **16**, 6521–6534 (1997).
15. Samach, A. et al. The UNUSUAL FLORAL ORGANS gene of *Arabidopsis thaliana* is an F-box protein required for normal patterning and growth in the floral meristem. *Plant J.* **20**, 433–445 (1999).
16. Simon, R., Carpenter, R., Doyle, S. & Coen, E. Fimbriata controls flower development by mediating between meristem and organ identity genes. *Cell* **78**, 99–107 (1994).
17. Wang, X. et al. The COP9 signalosome interacts with SCF UFO and participates in *Arabidopsis* flower development. *Plant Cell* **15**, 1071–1082 (2003).
18. Chae, E., Tan, Q. K.-G., Hill, T. A. & Irish, V. F. An *Arabidopsis* F-box protein acts as a transcriptional co-factor to regulate floral development. *Development* **135**, 1235–1245 (2008).
19. Geng, F., Wenzel, S. & Tansey, W. P. Ubiquitin and proteasomes in transcription. *Annu. Rev. Biochem.* **81**, 177–201 (2012).
20. Risseeuw, E. et al. An activated form of UFO alters leaf development and produces ectopic floral and inflorescence meristems. *PLoS ONE* **8**, e83807 (2013).
21. Krizek, B. A., Lewis, M. W. & Fletcher, J. C. RABBIT EARS is a second-whorl repressor of AGAMOUS that maintains spatial boundaries in *Arabidopsis* flowers. *Plant J.* **45**, 369–383 (2006).
22. Busch, M. A., Bomblies, K. & Weigel, D. Activation of a floral homeotic gene in *Arabidopsis*. *Science* **285**, 585–587 (1999).
23. Hill, T. A., Day, C. D., Zondlo, S. C., Thackeray, A. G. & Irish, V. F. Discrete spatial and temporal cis-acting elements regulate transcription of the *Arabidopsis* floral homeotic gene APETALA3. *Development* **125**, 1711–1721 (1998).
24. Lamb, R. S., Hill, T. A., Tan, Q. K.-G. & Irish, V. F. Regulation of APETALA3 floral homeotic gene expression by meristem identity genes. *Development* **129**, 2079–2086 (2002).
25. Goslin, K. et al. Transcription factor interplay between LEAFY and APETALA1/CAULIFLOWER during floral initiation. *Plant Physiol.* **174**, 1097–1109 (2017).
26. Sayou, C. et al. A SAM oligomerization domain shapes the genomic binding landscape of the LEAFY transcription factor. *Nat. Commun.* **7**, 11222 (2016).
27. Weigel, D., Alvarez, J., Smyth, D. R., Yanofsky, M. F. & Meyerowitz, E. M. LEAFY controls floral meristem identity in *Arabidopsis*. *Cell* **69**, 843–859 (1992).
28. Weigel, D. & Nilsson, O. A developmental switch sufficient for flower initiation in diverse plants. *Nature* **377**, 495–500 (1995).
29. Hamès, C. et al. Structural basis for LEAFY floral switch function and similarity with helix-turn-helix proteins. *EMBO J.* **27**, 2628–2637 (2008).
30. Sayou, C. et al. A promiscuous intermediate underlies the evolution of LEAFY DNA binding specificity. *Science* **343**, 645–648 (2014).
31. Zhao, D., Yu, Q., Chen, M. & Ma, H. The ASK1 gene regulates B function gene expression in cooperation with UFO and LEAFY in *Arabidopsis*. *Development* **128**, 2735–2746 (2001).
32. Ni, W. et al. Regulation of flower development in *Arabidopsis* by SCF complexes. *Plant Physiol.* **134**, 1574–1585 (2004).
33. Levin, J. Z., Fletcher, J. C., Chen, X. & Meyerowitz, E. M. A genetic screen for modifiers of UFO meristem activity identifies three novel FUSED FLORAL ORGANS genes required for early flower development in *Arabidopsis*. *Genetics* **149**, 579–595 (1998).
34. Singh, N. & Bhalla, N. Moonlighting Proteins. *Annu. Rev. Genet.* **54**, 265–285 (2020).
35. Honma, T. & Goto, K. The *Arabidopsis* floral homeotic gene PISTILLATA is regulated by discrete cis-elements responsive to induction and maintenance signals. *Development* **127**, 2021–2030 (2000).
36. Tilly, J. J., Allen, D. W. & Jack, T. The CArG boxes in the promoter of the *Arabidopsis* floral organ identity gene APETALA3 mediate diverse regulatory effects. *Development* **125**, 1647–1657 (1998).
37. Liu, C., Xi, W., Shen, L., Tan, C. & Yu, H. Regulation of floral patterning by flowering time genes. *Dev. Cell* **16**, 711–722 (2009).
38. Gregis, V., Sessa, A., Colombo, L. & Kater, M. M. AGL24, SHORT VEGETATIVE PHASE, and APETALA1 redundantly control AGAMOUS during early stages of flower development in *Arabidopsis*. *Plant Cell* **18**, 1373–1382 (2006).
39. Castillejo, C., Romera-Branchat, M. & Pelaz, S. A new role of the *Arabidopsis* SEPALLATA3 gene revealed by its constitutive expression. *Plant J.* **43**, 586–596 (2005).
40. Siggers, T., Duyzend, M. H., Reddy, J., Khan, S. & Bulyk, M. L. Non-DNA-binding cofactors enhance DNA-binding specificity of a transcriptional regulatory complex. *Mol. Syst. Biol.* **7**, 555 (2011).
41. Babb, R., Huang, C., Aufiero, D. J. & Herr, W. DNA recognition by the herpes simplex virus transactivator VP16: a novel DNA-binding structure. *Mol. Cell. Biol.* **21**, 4700–4712 (2001).
42. Chahtane, H. et al. LEAFY activity is post-transcriptionally regulated by BLADE ON PETIOLE2 and CULLIN3 in *Arabidopsis*. *N. Phytol.* **220**, 579–592 (2018).
43. Blanvillain, R. et al. The *Arabidopsis* peptide kiss of death is an inducer of programmed cell death. *EMBO J.* **30**, 1173–1183 (2011).
44. Takeda, S., Matsumoto, N. & Okada, K. RABBIT EARS, encoding a SUPERMAN-like zinc finger protein, regulates petal development in *Arabidopsis thaliana*. *Development* **131**, 425–434 (2004).

45. Benlloch, R. et al. Integrating long-day flowering signals: a LEAFY binding site is essential for proper photoperiodic activation of APETALA1. *Plant J.* **67**, 1094–1102 (2011).
46. Iwata, Y., Lee, M. H. & Koizumi, N. Analysis of a transcription factor using transient assay in *Arabidopsis* protoplasts. *Methods Mol. Biol.* **754**, 107–117 (2011).
47. Dümmeler, A., Lawrence, A. M. & de Marco, A. Simplified screening for the detection of soluble fusion constructs expressed in *E. coli* using a modular set of vectors. *Microb. Cell Fact.* **4**, 34 (2005).
48. Lai, X. et al. The LEAFY floral regulator displays pioneer transcription factor properties. *Mol. Plant* **14**, 829–837 (2021).
49. Bartlett, A. et al. Mapping genome-wide transcription-factor binding sites using DAP-seq. *Nat. Protoc.* **12**, 1659–1672 (2017).
50. Cutler, S. R., Ehrhardt, D. W., Griffitts, J. S. & Somerville, C. R. Random GFP::cDNA fusions enable visualization of subcellular structures in cells of *Arabidopsis* at a high frequency. *Proc. Natl Acad. Sci. USA* **97**, 3718–3723 (2000).
51. Chahtane, H. et al. A variant of LEAFY reveals its capacity to stimulate meristem development by inducing RAX1. *Plant J.* **74**, 678–689 (2013).
52. Punjani, A., Rubinstein, J. L., Fleet, D. J. & Brubaker, M. A. cryoSPARC: algorithms for rapid unsupervised cryo-EM structure determination. *Nat. Methods* **14**, 290–296 (2017).
53. Wagner, T. et al. SPHIRE-crYOLO is a fast and accurate fully automated particle picker for cryo-EM. *Commun. Biol.* **2**, 218 (2019).
54. Punjani, A., Zhang, H. & Fleet, D. J. Non-uniform refinement: adaptive regularization improves single-particle cryo-EM reconstruction. *Nat. Methods* **17**, 1214–1221 (2020).
55. Sanchez-Garcia, R. et al. DeepEMhancer: a deep learning solution for cryo-EM volume post-processing. *Commun. Biol.* **4**, 874 (2021).
56. Pettersen, E. F. et al. UCSF Chimera—a visualization system for exploratory research and analysis. *J. Comput. Chem.* **25**, 1605–1612 (2004).
57. Pettersen, E. F. et al. UCSF ChimeraX: structure visualization for researchers, educators, and developers. *Protein Sci.* **30**, 70–82 (2021).
58. Emsley, P., Lohkamp, B., Scott, W. G. & Cowtan, K. Features and development of Coot. *Acta Crystallogr. D Biol. Crystallogr.* **66**, 486–501 (2010).
59. Afonine, P. V. et al. Real-space refinement in PHENIX for cryo-EM and crystallography. *Acta Crystallogr. D Struct. Biol.* **74**, 531–544 (2018).
60. Jumper, J. et al. Highly accurate protein structure prediction with AlphaFold. *Nature* **596**, 583–589 (2021).
61. Terwilliger, T. C. et al. Improved AlphaFold modeling with implicit experimental information. *Nat. Methods* **19**, 1376–1382 (2022).
62. Lai, X. et al. Genome-wide binding of SEPALLATA3 and AGAMOUS complexes determined by sequential DNA-affinity purification sequencing. *Nucleic Acids Res.* **48**, 9637–9648 (2020).
63. Gaspar, J. M. NGmerge: merging paired-end reads via novel empirically-derived models of sequencing errors. *BMC Bioinform.* **19**, 536 (2018).
64. Berardini, T. Z. et al. The *Arabidopsis* Information Resource: making and mining the ‘gold standard’ annotated reference plant genome. *Genesis* **53**, 474–485 (2015).
65. Jalili, V., Matteucci, M., Masseroli, M. & Morelli, M. J. Using combined evidence from replicates to evaluate ChIP-seq peaks. *Bioinformatics* **31**, 2761–2769 (2015).
66. Machanick, P. & Bailey, T. L. MEME-ChIP: motif analysis of large DNA datasets. *Bioinformatics* **27**, 1696–1697 (2011).
67. Stigliani, A. et al. Capturing auxin response factors syntax using DNA binding models. *Mol. Plant* **12**, 822–832 (2019).
68. Moyroud, E. et al. Prediction of regulatory interactions from genome sequences using a biophysical model for the *Arabidopsis* LEAFY transcription factor. *Plant Cell* **23**, 1293–1306 (2011).
69. Sachs, M. C. plotROC: A Tool for Plotting ROC Curves. *J. Stat. Softw.* **79**, 1–19 (2017)..
70. Schmid, M. et al. A gene expression map of *Arabidopsis thaliana* development. *Nat. Genet.* **37**, 501–506 (2005).
71. Wu, J. et al. gcrma: Background Adjustment Using Sequence Information. R package version 2.70.0. (2022). <https://bioconductor.org/packages/release/bioc/manuals/gcrma/man/gcrma.pdf>
72. Ritchie, M. E. et al. limma powers differential expression analyses for RNA-sequencing and microarray studies. *Nucleic Acids Res.* **43**, e47 (2015).
73. Jin, R. et al. LEAFY is a pioneer transcription factor and licenses cell reprogramming to floral fate. *Nat. Commun.* **12**, 626 (2021).
74. Quinlan, A. R. & Hall, I. M. BEDTools: a flexible suite of utilities for comparing genomic features. *Bioinformatics* **26**, 841–842 (2010).
75. RStudio Team RStudio: Integrated Development for R. (RStudio, PBC, Boston, MA, 2020). <http://www.rstudio.com/>
76. Gagne, J. M., Downes, B. P., Shiu, S. H., Durski, A. M. & Vierstra, R. D. The F-box subunit of the SCF E3 complex is encoded by a diverse superfamily of genes in *Arabidopsis*. *Proc. Natl Acad. Sci. USA* **99**, 11519–11524 (2002).
77. Zhang, S. et al. Proliferating floral organs (pfo), a *Lotus japonicus* gene required for specifying floral meristem determinacy and organ identity, encodes an F-box protein. *Plant J.* **33**, 607–619 (2003).
78. Zhao, Y. et al. Evolutionary co-option of floral meristem identity genes for patterning of the flower-like Asteraceae inflorescence. *Plant Physiol.* **172**, 284–296 (2016).
79. Chen, Y. et al. CsUFO is involved in the formation of flowers and tendrils in cucumber. *Theor. Appl. Genet.* **3**, 2141–2150 (2021).
80. Ikeda, K., Ito, M., Nagasawa, N., Kyozuka, J. & Nagato, Y. Rice ABERRANT PANICLE ORGANIZATION 1, encoding an F-box protein, regulates meristem fate. *Plant J.* **51**, 1030–1040 (2007).
81. Li, F. et al. Reduced expression of CbUFO is associated with the phenotype of a flower-defective *Cosmos bipinnatus*. *Int. J. Mol. Sci.* **20**, 2503 (2019).
82. Sasaki, K. et al. Mutation in *Torenia fournieri* Lind. UFO homolog confers loss of TfLFY interaction and results in a petal to sepal transformation. *Plant J.* **71**, 1002–1014 (2012).
83. Sharma, B. et al. Homologs of LEAFY and UNUSUAL FLORAL ORGANS promote the transition from inflorescence to floral meristem identity in the cymose *Aquilegia coerulea*. *Front. Plant Sci.* **10**, 1218 (2019).
84. Taylor, S., Hofer, J. & Murfet, I. Stamina pistilloida, the pea ortholog of Fim and UFO, is required for normal development of flowers, inflorescences, and leaves. *Plant Cell* **13**, 31–46 (2001).
85. Ashkenazy, H. et al. ConSurf 2016: an improved methodology to estimate and visualize evolutionary conservation in macromolecules. *Nucleic Acids Res.* **44**, W344–W350 (2016).

## Acknowledgements

We thank A. M. Boisson for preparing the suspension cells, X. Lai for the ampDAP-seq libraries and technical assistance and R. Koes for sharing data and materials. We acknowledge C. Marondedze, G. Vachon, M. Le Masson, C. Berthollet, B. Orlando Marchesano and J. Bourenane-Vieira for help with the experiments. We thank G. Vert, U. Dolde and R. Dumas for discussion. The electron microscopy facility is supported by the Rhône-Alpes Region, the FRM, the FEDER and the GIS-IBISA. This work used the platforms of the Grenoble Instruct-ERIC

centre (ISBG; UAR 3518 CNRS-CEA-UGA-EMBL) within the Grenoble Partnership for Structural Biology, supported by FRISBI (ANR-10-INBS-0005-02). We thank C. Mas for assistance and access to the biophysical platform. This work was supported by the GRAL Labex financed within the University Grenoble Alpes graduate school (Ecoles Universitaires de Recherche) CBH-EUR-GS (ANR-17-EURE-0003), the CEA (PhD fellowship to P.R.) and the ANR-17-CE20-0014-01 Ubiflor project to F.P.

## Author contributions

F.P. and P.R. designed the project. P.R. performed the plant experiments with assistance from G.T. P.R. and E.T. performed the biochemical experiments with assistance from H.C. on the evolutionary analyses. L.T. performed the bioinformatics analyses with assistance from J.L. and R.B.-M. E.Z. and G.S. performed the cryo-EM experiments, and M.N., E.Z., C.Z. and G.S. analysed the data. P.R. and L.T. assembled the figures. P.R. and F.P. wrote the paper with contributions from L.T. and C.Z.

## Competing interests

The authors declare no competing interests.

## Additional information

**Extended data** is available for this paper at

<https://doi.org/10.1038/s41477-022-01336-2>.

**Supplementary information** The online version contains supplementary material available at <https://doi.org/10.1038/s41477-022-01336-2>.

**Correspondence and requests for materials** should be addressed to François Parcy.

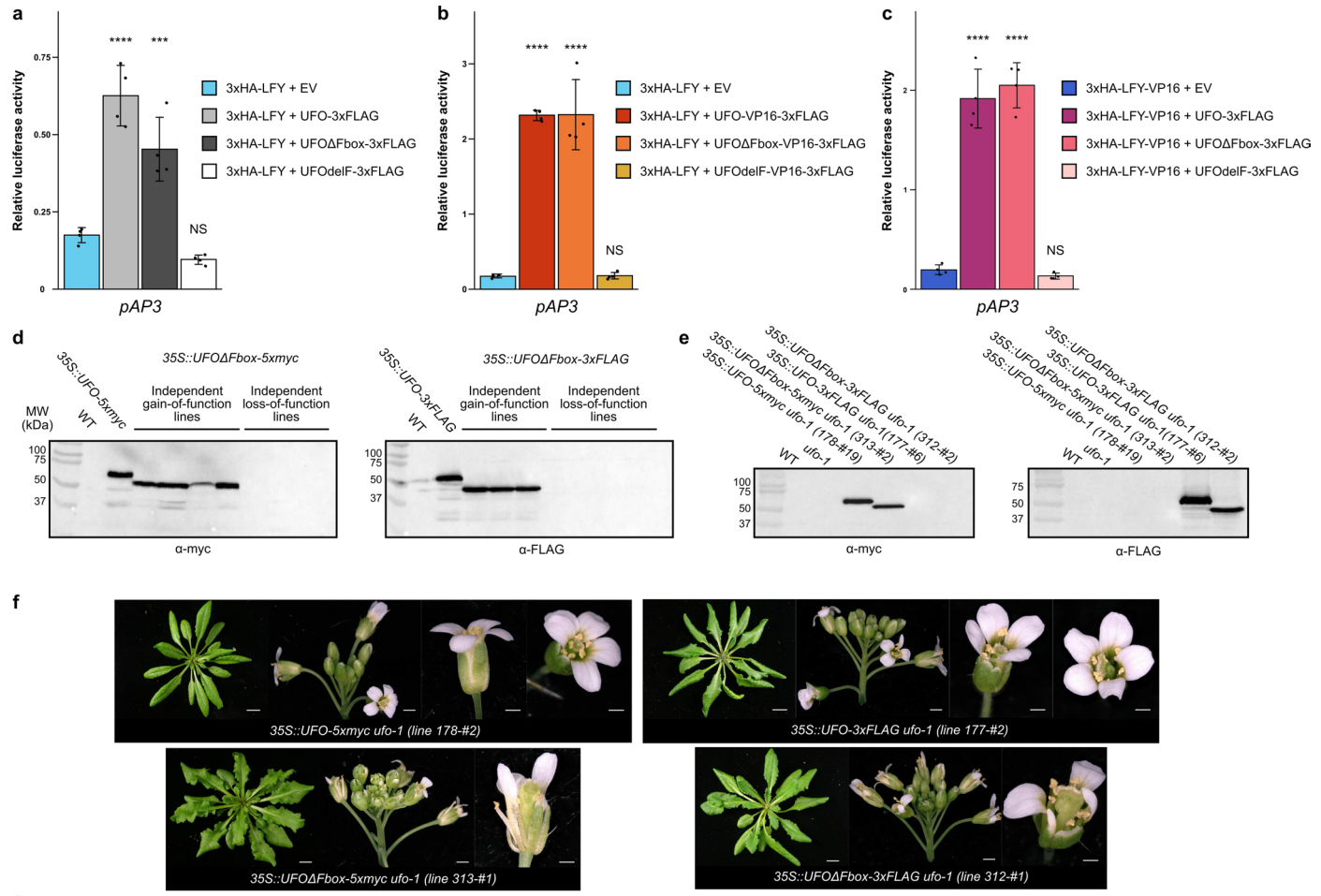
**Peer review information** *Nature Plants* thanks Nobutoshi Yamaguchi, Aiwu Dong and the other, anonymous, reviewer(s) for their contribution to the peer review of this work.

**Reprints and permissions information** is available at [www.nature.com/reprints](http://www.nature.com/reprints).

**Publisher's note** Springer Nature remains neutral with regard to jurisdictional claims in published maps and institutional affiliations.

Springer Nature or its licensor (e.g. a society or other partner) holds exclusive rights to this article under a publishing agreement with the author(s) or other rightsholder(s); author self-archiving of the accepted manuscript version of this article is solely governed by the terms of such publishing agreement and applicable law.

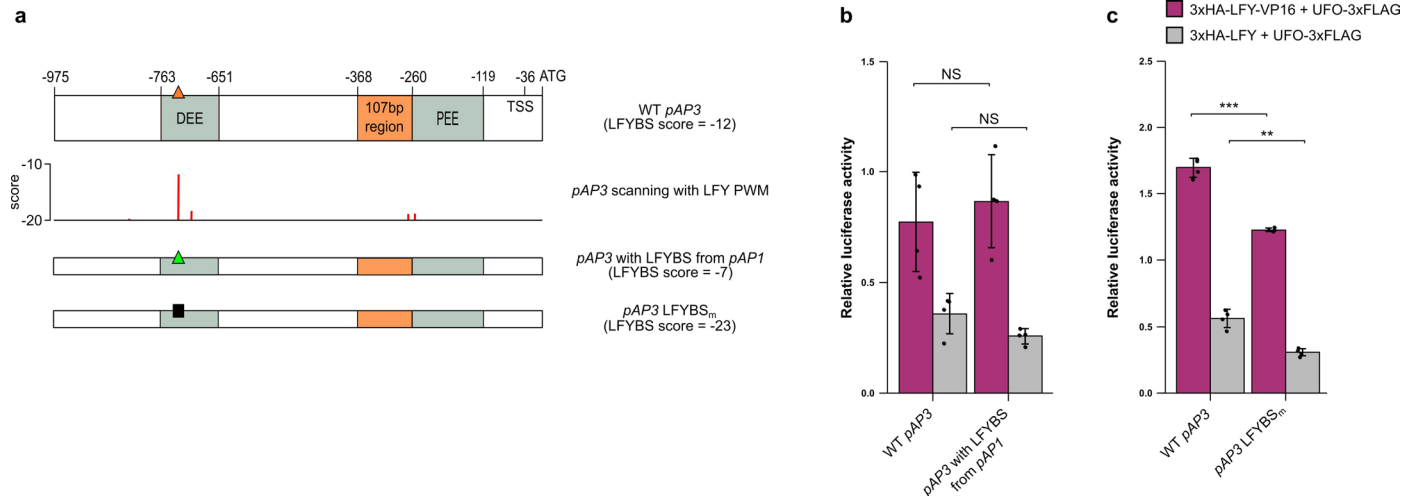
© The Author(s), under exclusive licence to Springer Nature Limited 2023



### Extended Data Fig. 1 | UFO has SCF-dependent and independent functions.

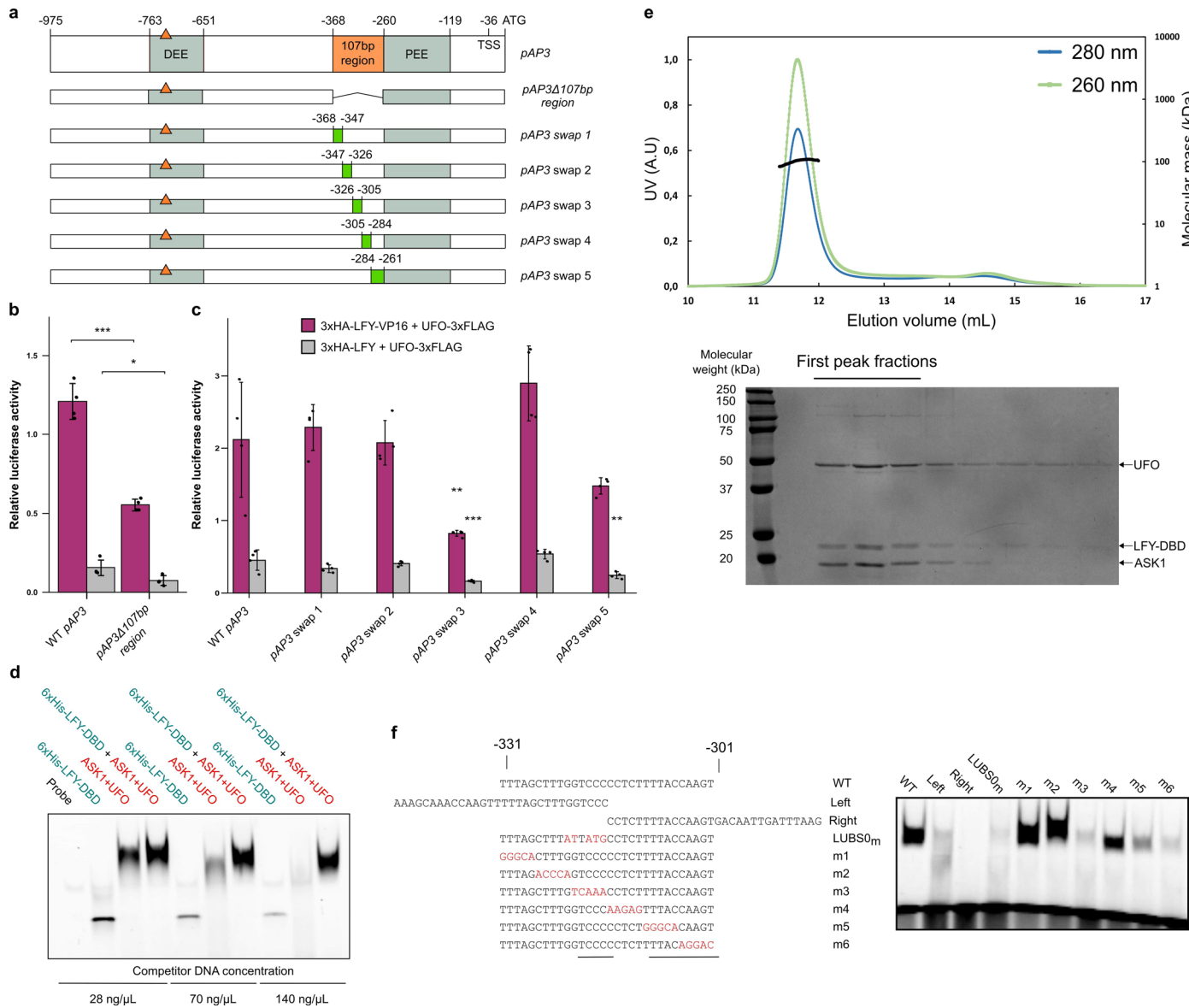
**a-c**, *pAP3* activation measured by DLRA in *Arabidopsis* protoplasts. EV = Empty Vector (pRT104-3xHA). UFOΔFbox corresponds to a deletion of the whole N-terminal part comprising the F-box domain (aa. 1-90), while UFOdelF corresponds to a previously-described internal deletion in the F-box domain (aa. 50-62)<sup>20</sup>. Data represent averages of independent biological replicates and are presented as mean  $\pm$  SD, each dot representing one biological replicate ( $n=4$ ). One-way ANOVA with Tukey's multiple comparisons tests. Stars above bars represent a significant statistical difference compared to 3xHA-LFY + EV or 3xHA-LFY-VP16 + EV negative controls (NS:  $p > 0.05$ ; \*:  $p < 0.05$ , \*\*:  $p < 0.01$ , \*\*\*:  $p < 0.001$  and \*\*\*\*:  $p < 0.0001$ ). **d**, Western Blot on protein extracts from independent T1 plants from different phenotypic classes described in Fig. 1g (one independent line per lane). 35S::UFO-5xmyc (line 178-#19) and 35S::UFO-3xFLAG (line 177-#6) plants were used as positive controls. Total proteins were extracted from rosette leaves. Note the difference of molecular weight between UFO and

UFOΔFbox. Loss-of-function defects are likely due to silencing of both transgene-encoded UFOΔFbox and endogenous UFO. **e**, Western Blot on protein extracts from F2 plants described in Fig. 1h. Total proteins were extracted from rosette leaves. **f**, *ufo-1* complementation assay with other 35S::UFO and 35S::UFOΔFbox lines. Rosette leaves (right, scale bar, 1 cm), inflorescence (middle, scale bar 1 mm) and flower (right, scale bar, 0.5 mm) phenotypes are shown. Primary inflorescences were removed to observe rosette phenotype. For each construct, at least 5 plants were analyzed per line. As in Risseeuw et al, our 35S::UFO lines displayed relatively milder phenotypes than the 35S::UFO phenotypes reported by Lee et al.<sup>6,20</sup>. Note that the 35S::UFO-5xmyc 178-#2 line did not display the serrated leaves phenotype. **g**, Sequence alignment of UFO N-terminal region. The F-box domain is represented<sup>70</sup>. In selected species, presented proteins were identified as UFO homologs and their role was confirmed genetically<sup>7,11,12,16,77-84</sup>. Source data are available in Supplementary Data 4.



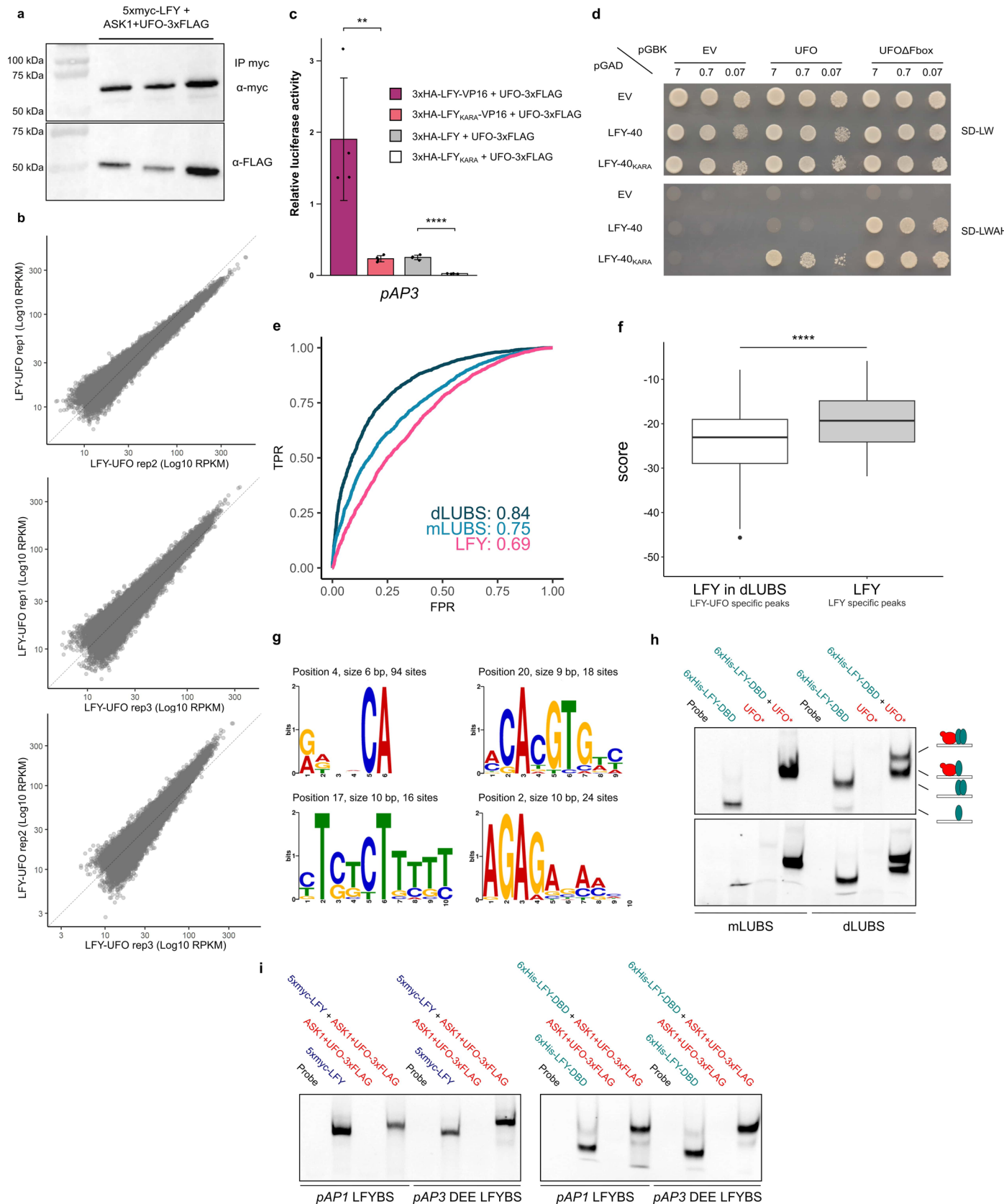
**Extended Data Fig. 2 | *pAP3* DEE LFYBS is not required for LFY-UFO-dependent *pAP3* activation.** **a**, Schematic representation of *pAP3*. Top row represents WT *pAP3* with regulatory regions and *cis*-elements. Orange triangle represents LFYBS. The second row represents the scores for the best LFYBS obtained by scanning WT *pAP3* sequence with LFY PWM<sup>68</sup> (the best binding sites correspond to the less negative score values). Other rows represent the different *pAP3* versions used in **(b)** and **(c)**. LFYBS mutation corresponds to the previously

described *site1m-site2m* mutation<sup>24</sup>. **b,c**, *pAP3* activation with promoter versions described in **(a)** and indicated effectors. For bar charts, data represent averages of independent biological replicates and are presented as mean  $\pm$  SD, each dot representing one biological replicate ( $n = 4$ ). Unpaired t-tests **(b,c)**. (NS:  $p > 0.05$ , \*:  $p < 0.05$ , \*\*:  $p < 0.01$ , \*\*\*:  $p < 0.001$ ). Source data are available in Supplementary Data 4.



**Extended Data Fig. 3 | Analysis of *pAP3* activation by LFY-UFO.** **a**, Description of *pAP3*. Top line represents WT *pAP3* with regulatory regions and *cis*-elements. Coordinates are relative to *AP3* start codon. TSS: Transcription Start Site. Orange triangle represents LFYBS. Other rows show the promoter versions used in (b) and (c). Green rectangles in swapped versions correspond to the same random sequence. **b,c**, *pAP3* LFY-UFO response element mapping with *pAP3* versions described in (a) by DLRA in Arabidopsis protoplasts. Data represent averages of independent biological replicates and are presented as mean  $\pm$  SD, each dot representing one biological replicate ( $n = 4$ ). One-way ANOVA with Tukey's multiple comparisons test (c). One-way ANOVA was performed with data from the same effector, and stars represent a statistical difference compared to WT *pAP3*. Unpaired t-tests (b). (NS:  $p > 0.05$ ; \*:  $p < 0.05$ ; \*\*:  $p < 0.01$ ; \*\*\*:  $p < 0.001$ ). **d**, EMSA with ASK1-UFO, LFY-DBD and LUBSO DNA probe. Different competitor DNA concentrations were tested as indicated. **e**, Molecular mass determination for ASK1-UFO-LFY-DBD in complex with LUBSO DNA by SEC-MALLS (top). Elution

profiles correspond to absorbance at 280 nm and 260 nm (left ordinate axis, A.U: Arbitrary Unit). The black line shows the molecular mass distribution (right ordinate axis). A mass of  $102 \pm 3.3$  kDa was found for this ASK1-UFO-LFY-DBD-LUBSO complex, consistent with one copy of each protein per DNA molecule (theoretical mass of 108 kDa). Coomassie-stained SDS-PAGE gel of the different SEC-MALLS fractions (bottom). Each lane corresponds to a 0.5 mL fraction. Molecular weights of the protein standards are indicated (BioRad Precision Plus). Faint bands above UFO likely correspond to contaminants. **f**, EMSA with ASK1-UFO, LFY-DBD and indicated DNA probes (right). Each DNA probe was mixed with the same ASK1-UFO-LFY-DBD protein mix. Note that the LUBSO mutation also reduced *pAP3* activation in protoplasts (Fig. 2b). Source data are available in Supplementary Data 4.

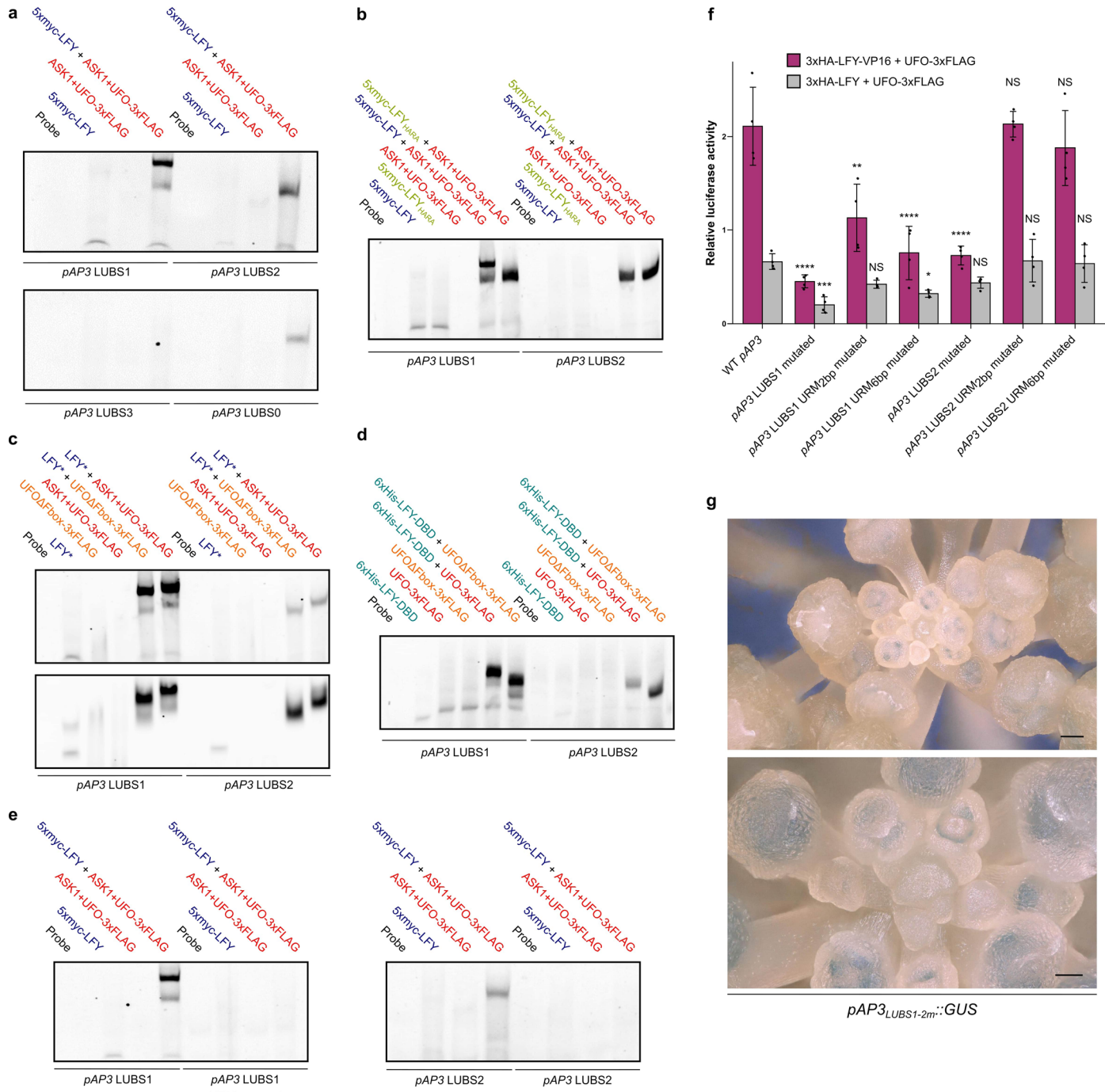


Extended Data Fig. 4 | See next page for caption.

**Extended Data Fig. 4 | Genome-wide analysis of LFY-UFO binding.** **a**, Western Blot after DNA elution during ampDAP-seq experiment. After DNA elution, 20 µL of 1X SDS-PAGE Protein Sample Buffer was added to the remaining beads to run WB. Each lane represents one replicate. **b**, Assessment of experimental reproducibility of ampDAP-seq experiment through the comparison of replicates datasets 2 by 2. **c**, Effect of the LFY KARA mutation (K303A-R233A)<sup>51</sup> on *pAP3* activation in Arabidopsis protoplasts. Data represent averages of independent biological replicates and are presented as mean ± SD, each dot representing one biological replicate ( $n = 4$ ). Unpaired t-tests (\*\*:  $p < 0.01$ ; \*\*\*\*:  $p < 0.0001$ ). **d**, The LFY KARA mutation (K303A-R233A) does not disrupt LFY-UFO interaction in Yeast-Two-Hybrid (Y2H). EV = Empty Vector. LFY-40 is a LFY version lacking the first 40 aa and better tolerated by yeast cells. Values correspond to the different dilutions (OD = 7, 0.7 and 0.07). Top picture corresponds to the non-selective plate lacking Leucine and Tryptophan (SD -L-W), and bottom picture to the selective plate lacking Leucine, Tryptophan, Histidine and Adenine (SD -L-W-A-H). Pictures were taken at day + 4. **e**, Receiver operating characteristics (ROC) curves for mLUBS, dLUBS and LFY using the top 20% high-CFC LFY-UFO-specific peaks. Area under the curve (AUC) values are shown. TPR: True Positive Rate, FPR: False Positive Rate. **f**, Score distribution of LFY PWM with dependencies<sup>68</sup> within dLUBS (best site on 20% most LFY-UFO-specific genomic regions, high

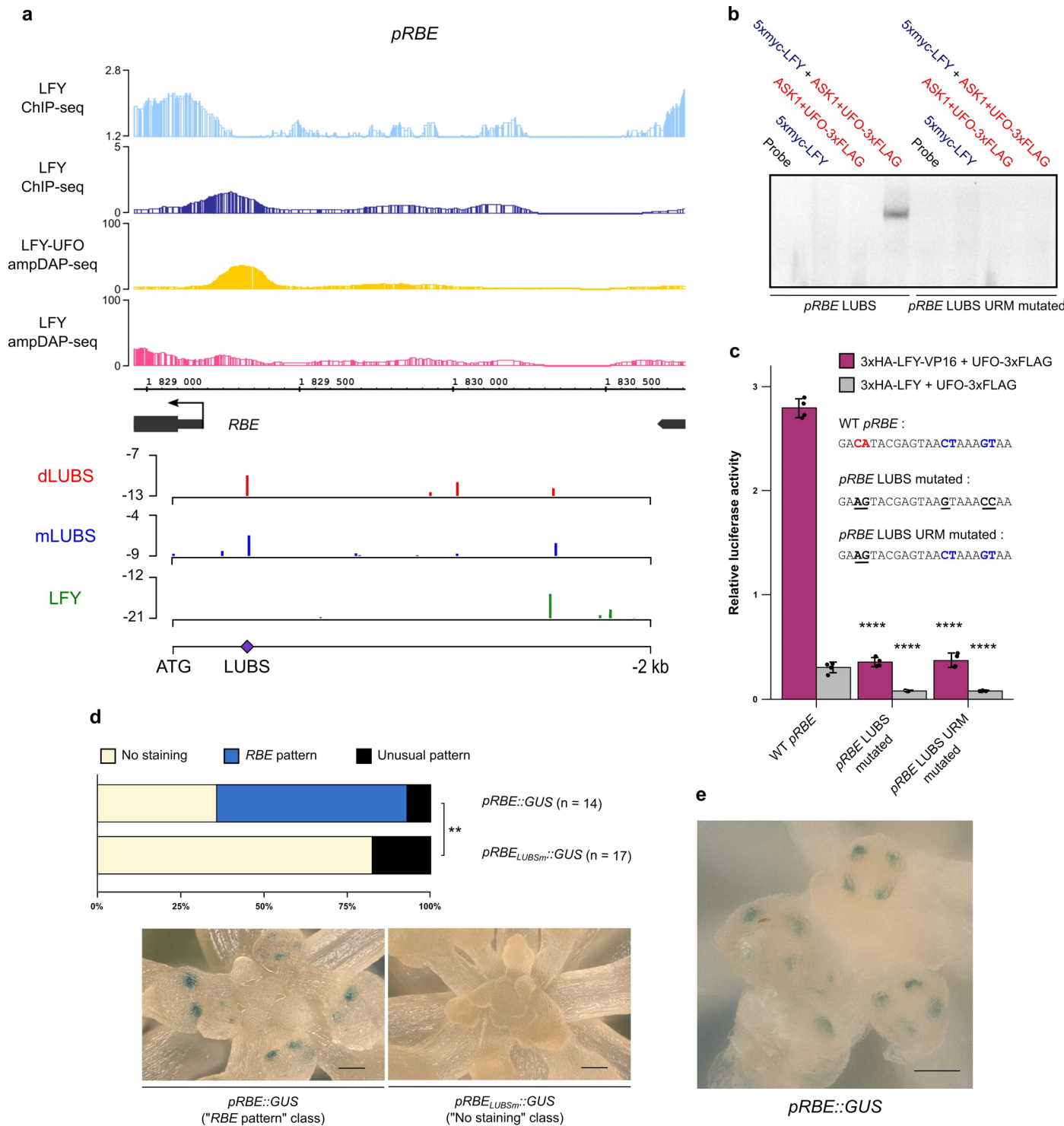
CFC,  $n = 3843$  genomic regions) and in canonical LFYBS (best site on 20% most LFY-specific genomic regions, low CFC,  $n = 3843$  genomic regions). Best sites were selected within ±25 bp around the peak maximum. Wilcoxon rank sum test (\*\*\*\*:  $p < 0.0001$ ). Median (solid line), interquartile range (box edges), ±1.5 × interquartile range (whiskers) and outliers (black dot) are shown.

**g**, *De novo* identification of URM from LFY ChIP-seq data<sup>25</sup>. Motifs identified at a fixed distance from LFY canonical binding sites in 298 regions harboring high LFY ChIP-seq to LFY ampDAP-seq coverage ratio. The text above each motif gives the motif's start position relative to the canonical LFYBS, its length and the number of sites used to build the motif. **h**, EMSA with mLUBS and dLUBS highest score sequences. 6xHis-LFY-DBD is recombinant. UFO\* refers to either recombinant ASK1-UFO-3xFLAG complex (top gel) or *in vitro* produced UFO-3xFLAG (bottom gel). Drawings represent the different types of complexes involving LFY-DBD (pale blue) and ASK1-UFO (red) on DNA. LFY-DBD binds as a monomer as previously reported<sup>29</sup>. The fact that *in vitro* produced UFO-3xFLAG shifts DNA in the presence of LFY indicates that ASK1 is not required for the UFO-LFY-DNA complex formation *in vitro*. **i**, EMSA with DNA probes corresponding to *pAP1* and *pAP3DEE* LFYBS and indicated proteins. Note that probes used here have the same length as those used to study LUBS. Source data are available in Supplementary Data 4.



**Extended Data Fig. 5 | pAP3 LUBS are required for LFY-UFO-dependent activation.** **a**, EMSA with indicated probes and proteins. LUBS3 is the third highest-score pAP3 LUBS. Because LUBS0 is bound with a lower affinity by LFY-UFO compared to LUBS1 and LUBS2, we then focused on LUBS1 and LUBS2. **b**, EMSA with pAP3 LUBS1 and LUBS2 DNA probes and indicated proteins. LFY<sub>H383A-R386A</sub> (LFY<sub>HARA</sub>) is a LFY mutated version affected in its ability to dimerize<sup>29,51</sup>. Note the absence of the complex with a slower mobility on LUBS1 with LFY<sub>HARA</sub>. **c**, EMSA with pAP3 LUBS1 and LUBS2 DNA probes and indicated proteins. LFY\* refers to either *in vitro*-produced 5xmyc-LFY (top) or recombinant 6xHis-LFY-DBD (bottom). Note the difference of complex size between UFO and UFOΔFbox. **d**, Same as in **c** except that *in vitro* produced UFO-3xFLAG and UFOΔFbox-3xFLAG were produced *in vitro*. Note that *in vitro* produced UFO-3xFLAG and UFOΔFbox-3xFLAG behave similarly as recombinant UFO versions. **e**, EMSA with indicated proteins and DNA probes corresponding to pAP3 LUBS1 (left) and LUBS2 (right), WT or with URM mutated. **f**, Promoter activation measured by

DLRA in Arabidopsis protoplasts with indicated effectors. Different promoter versions were tested as indicated under x-axis. Either 2 bp (high-informative CA) or 6 bp (whole URM) of pAP3 LUBS1 and LUBS2 URM were mutated. Data represent averages of independent biological replicates and are presented as mean  $\pm$  SD, each dot representing one biological replicate ( $n = 4$ ). One-way ANOVA with Tukey's multiple comparisons tests. One-way ANOVA were performed with data from the same effector and stars represent a statistical difference compared to WT pAP3 promoter. (NS:  $p > 0.05$ , \*:  $p < 0.05$ , \*\*:  $p < 0.01$ , \*\*\*:  $p < 0.001$  and \*\*\*\*:  $p < 0.0001$ ). **g**, *In vivo* analysis of pAP3<sub>LUBS1-2m</sub>::GUS fusions. Same as in Fig. 3d, except that staining incubation time was increased to 17 h (4 h incubation in Fig. 3d). Representative pictures are shown (top scale bar, 100  $\mu$ m, bottom scale bar, 50  $\mu$ m). The faint AP3 pattern suggests that other LUBS (such as LUBS0) may take over but less efficiently. Note that with this staining incubation time, all plants expressing pAP3::GUS showed a highly saturated staining. Source data are available in Supplementary Data 4.

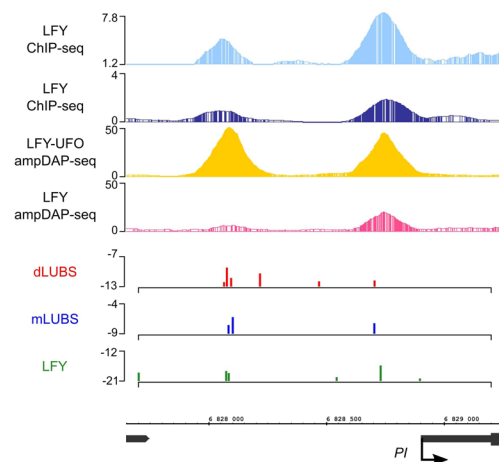
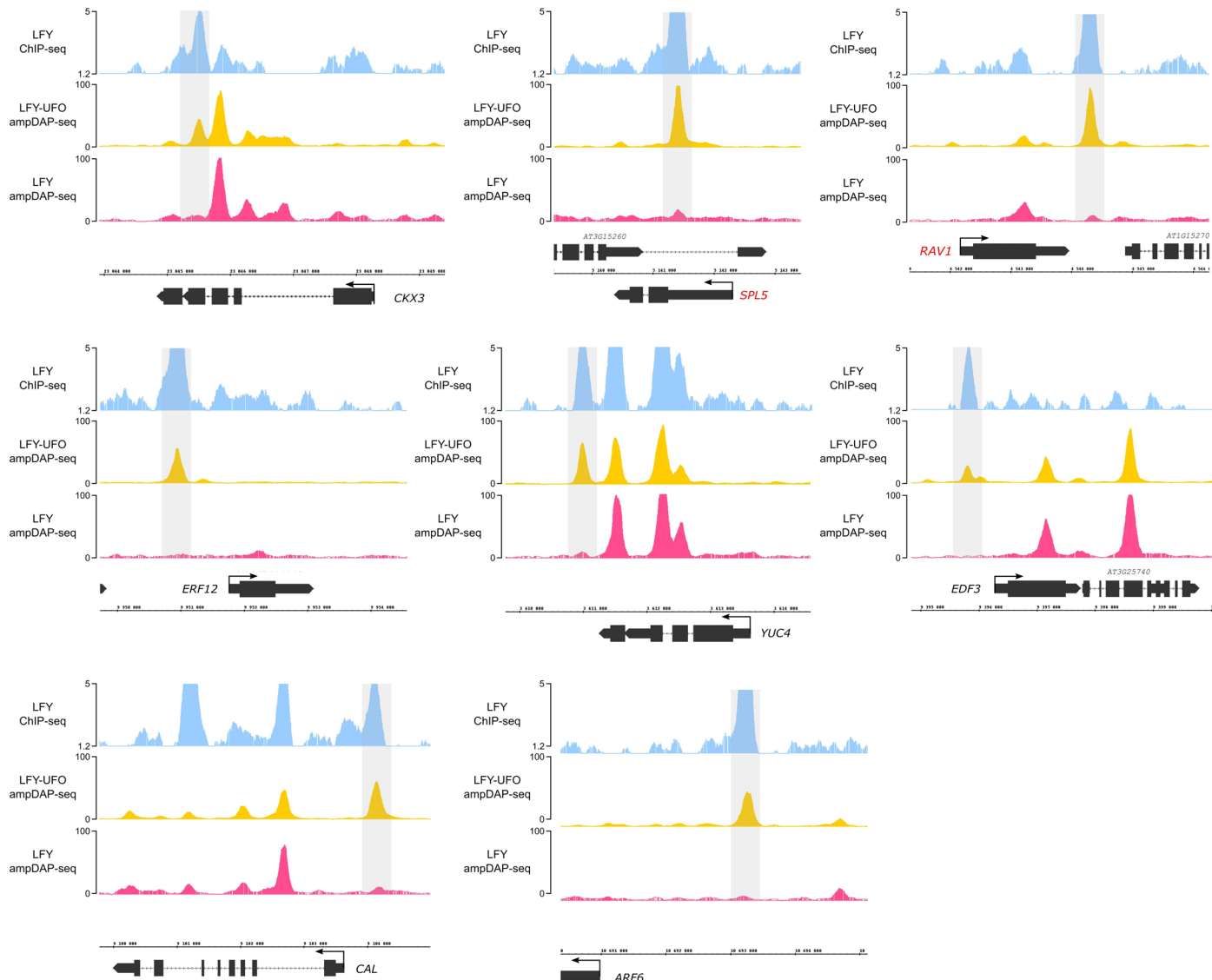


**Extended Data Fig. 6 | *pRBE* LUBS is required for LFY-UFO-dependent activation.** **a**, IGB view of *pRBE* showing LFY ChIP-seq in inflorescences (light blue)<sup>25</sup> or seedlings (dark blue)<sup>26</sup>, LFY-UFO ampDAP-seq (yellow), LFY ampDAP-seq (pink)<sup>48</sup>, numbers indicate read number range (top). Identification of LUBS in *pRBE* (bottom). Predicted binding sites using dLUBS and mLUBS models from Fig. 2e and LFY PWM with dependencies<sup>68</sup>, y-axis represents score values (bottom). The best binding sites correspond to the less negative score values. Studied LUBS is indicated with a purple square. **b**, EMSA with probes corresponding to *pRBE* LUBS, WT or with URM mutated. **c**, *pRBE* activation in *Arabidopsis* protoplasts. Effect of mutations (underlined) in URM (red) and in LFYBS (blue) bases of *pRBE* LUBS were assayed. Data represent averages of independent biological replicates and are presented as mean  $\pm$  SD,

each dot representing one biological replicate (n = 4). One-way ANOVA with Tukey's multiple comparisons test. One-way ANOVA were performed with data from the same effector, and stars represent a statistical difference compared to WT promoters (\*\*\*\*: p < 0.0001). **d**, *In vivo* analysis of *pRBE::GUS* fusions. The percentage of transgenic lines with RBE pattern, unusual pattern or absence of staining was scored (top;  $\chi^2$  test, \*\*: p < 0.01). n = number of independent lines. Unusual pattern refers to staining in unexpected tissues, each pattern seen in a single line. Representative pictures of plants with no staining (bottom left) and a RBE pattern (bottom right) are shown (scale bar, 50  $\mu$ m). **e**, *In vivo* analysis of *pRBE::GUS* fusions. Same as in (d), with another view showing staining in the four petal primordia (scale bar, 50  $\mu$ m). Source data are available in Supplementary Data 4.

**a**

Gene	Name	Description	Up/Down regulated	LFY ChIP-Seq set
AT1G13260	RAV1	related to ABI3/VP1 1	down	A
AT1G24530	NA	Transducin/WD40 repeat-like superfamily protein	down	B
AT1G34110	NA	Leucine-rich receptor-like protein kinase family protein	up	C; B
AT1G54010	NA	GDSL-like Lipase/Acylhydrolase superfamily protein	down	A
AT1G73805	NA	Calmodulin binding protein-like	down	C; B; A
AT1G74440	NA	Protein of unknown function (DUF962)	down	A
AT1G75450	ATCKX5	cytokinin oxidase 5	up	C; B; D
AT1G76110	NA	HMG (high mobility group) box protein with ARID/BRIGHT DNA-binding domain	up	A
AT1G80840	ATWRKY40	WRKY DNA-binding protein 40	up	C; B; A
AT3G15270	SPL5	squamosa promoter binding protein-like 5	up	A
AT3G20810	NA	2-oxoglutarate (2OG) and Fe(II)-dependent oxygenase superfamily protein	up	A
AT3G28180	ATCSLC04	Cellulose-synthase-like C4	down	B
AT3G54340	AP3	K-box region and MADS-box transcription factor family protein	up	B
AT3G55560	AGF2	AT-hook protein of GA feedback 2	up	C; B; A
AT4G00730	ANL2	Homeobox-leucine zipper family protein / lipid-binding START domain-containing protein	up	A
AT4G02380	AILAE5	senescence-associated gene 21	down	B
AT4G34160	CYCD3	CYCLIN D3	up	A
AT4G35900	FD	Basic-leucine zipper (bZIP) transcription factor family protein	down	C; B; A
AT5G02540	NA	NAD(P)-binding Rossmann-fold superfamily protein	up	B; D
AT5G20240	PI	K-box region and MADS-box transcription factor family protein	up	A

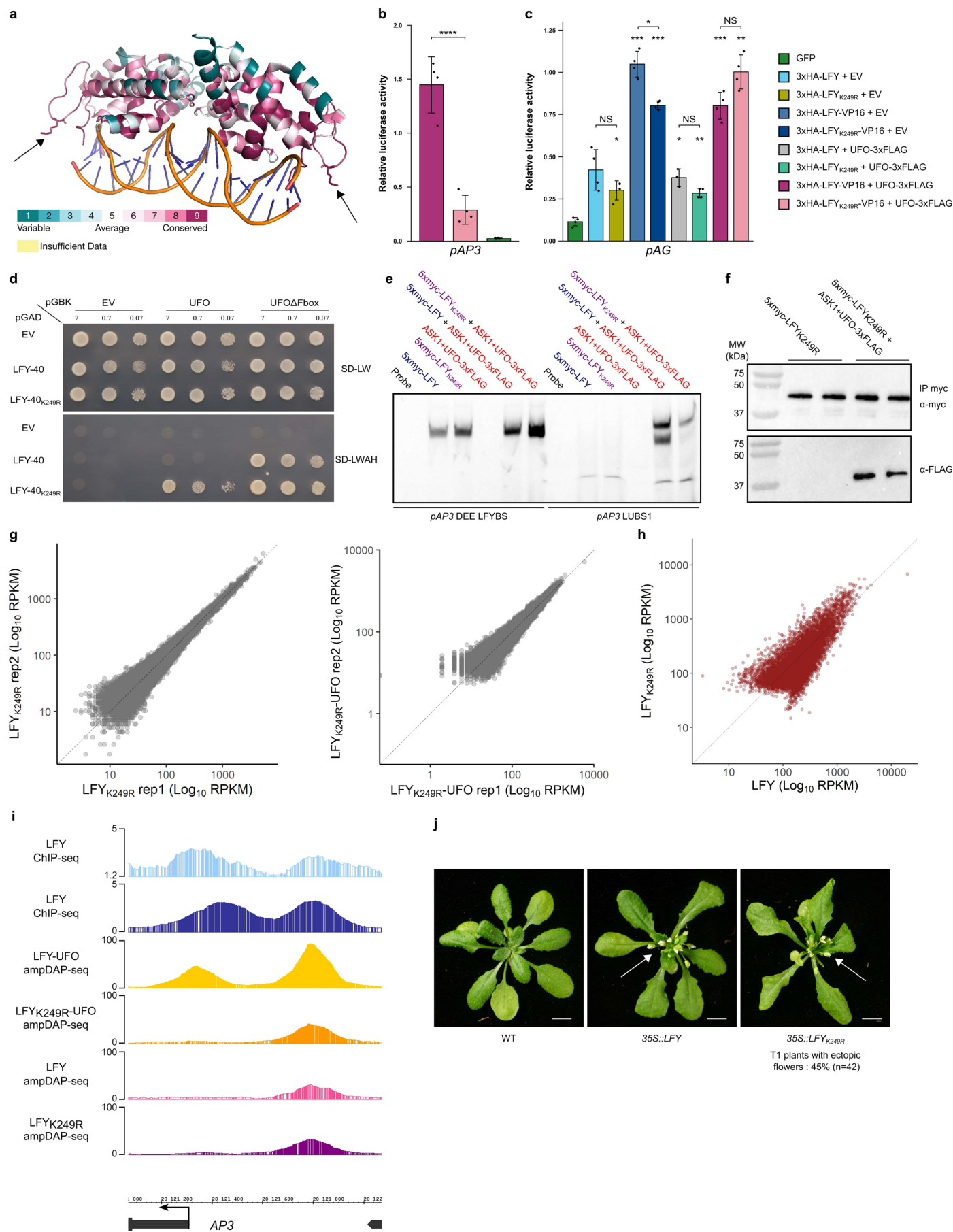
**b****c**

Extended Data Fig. 7 | See next page for caption.

**Extended Data Fig. 7 | LFY and UFO likely regulate other genes in *Arabidopsis*.**

**a.** List of candidate LFY-UFO target genes selected as i) present in regions specifically bound by LFY-UFO in ampDAP-seq (high CFC) ii) bound *in vivo* in LFY ChIP-seq experiments (A<sup>25</sup>; B<sup>26</sup>; C<sup>68</sup>; D<sup>73</sup>) and iii) deregulated in *ufo* inflorescences<sup>70</sup>. **b.** IGB view of *PISTILLATA* promoter region showing LFY ChIP-seq in inflorescences (light blue)<sup>25</sup> or seedlings (dark blue)<sup>26</sup>, LFY-UFO ampDAP-seq (yellow), LFY ampDAP-seq (pink)<sup>48</sup>, numbers indicate read number

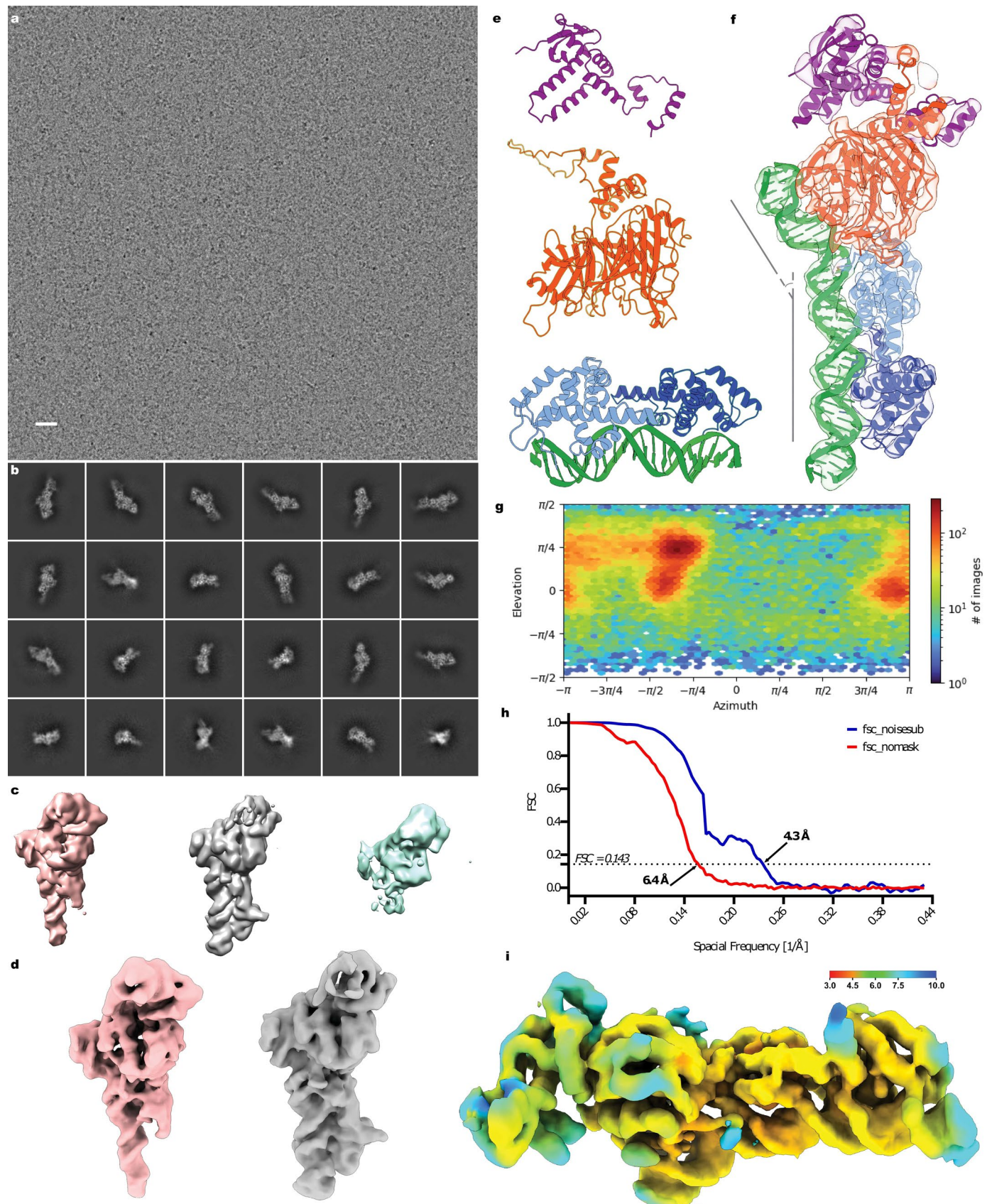
range (top). Predicted binding sites using the dLUBS, mLUBS models from Fig. 2e and LFY PWM with dependencies<sup>68</sup>, y-axis represents score values (bottom). **c.** IGB view of selected genes showing LFY ChIP-seq in inflorescences (light blue)<sup>25</sup>, LFY-UFO ampDAP-seq (yellow), LFY ampDAP-seq (pink)<sup>48</sup>, numbers indicate read number range. Genes in red are deregulated in *ufo* inflorescences<sup>70</sup>. ChIP-seq peaks better explained by LFY-UFO than by LFY alone are shaded in grey. Source data are available in Supplementary Data 4.



Extended Data Fig. 8 | See next page for caption.

**Extended Data Fig. 8 | The LFY K249 is essential for LFY-UFO-LUBS complex formation.** **a**, Structure of LFY-DBD<sup>29</sup>. Residues were colored by conservation using Consurf with default parameters<sup>35</sup>. K249 residues on each LFY monomer are represented as sticks and indicated with arrows. Note that the K249-containing loop is highly conserved. **b,c**, Promoter activation measured by DLRA in Arabidopsis protoplasts with indicated effectors (right). EV = Empty Vector (pRT104-3xHA). Tested promoters are indicated below each graph. Note that for 3xHA-LFY + UFO-3xFLAG on *pAG* only  $n = 3$  biological replicates are shown. Data represent averages of independent biological replicates and are presented as mean  $\pm$  SD, each dot representing one biological replicate ( $n = 4$  unless specified). One-way ANOVA with Tukey's multiple comparisons tests (**b**) or Welch's ANOVA with Games-Howell post-hoc test (**c**). In (**c**), stars above bars represent a statistical difference compared to GFP. Other comparisons are indicated with brackets. (NS:  $p > 0.05$ ; \*:  $p < 0.05$ , \*\*:  $p < 0.01$ , \*\*\*:  $p < 0.001$  and \*\*\*\*:  $p < 0.0001$ ). **d**, Effect of the LFY<sub>K249R</sub> mutation on LFY-UFO interaction in Y2H. EV = Empty Vector. LFY-40 is a LFY version lacking the first 40 aa and better tolerated by yeast cells. Values correspond to the different dilutions (OD = 7, 0.7 and 0.07). Top picture corresponds to the non-selective plate lacking Leucine and Tryptophan (SD-L-W), and bottom picture corresponds to the selective plate

lacking Leucine, Tryptophan, Histidine and Adenine (SD-L-W-A-H). Pictures were taken at day + 4. **e**, EMSA with DNA probes corresponding to *pAP3*DEE LFYBS and *pAP3*LUBS1 and indicated proteins. *pAP3*DEE LFYBS DNA probe was used as a control for binding on canonical LFYBS. **f**, WB after DNA elution during ampDAP-seq experiment. After DNA elution, 20  $\mu$ L of 1X SDS-PAGE Protein Sample Buffer was added to the remaining beads to run WB. Each lane represents one replicate. **g**, Reproducibility of ampDAP-seq experiments with LFY<sub>K249R</sub> (left) and LFY<sub>K249R</sub>-UFO (right) through the comparison of replicates datasets 2 by 2. **h**, Comparison of peak coverage in LFY<sub>K249R</sub> (y-axis, this study) and LFY (x-axis)<sup>48</sup> ampDAP-seq experiments. **i**, Integrated Genome Browser (IGB) view of *pAP3* showing LFY ChIP-seq in inflorescences (light blue)<sup>25</sup> or seedlings (dark blue)<sup>26</sup>, LFY-UFO ampDAP-seq (yellow; this study), LFY ampDAP-seq (pink)<sup>48</sup> and LFY<sub>K249R</sub> ampDAP-seq (purple; this study). Numbers indicate read number range. **j**, Pictures of WT and representative transgenic plants expressing *3SS::LFY* or *3SS::LFY<sub>K249R</sub>* (scale bar, 1 cm). The white arrows indicate ectopic rosette flowers. *3SS::LFY* was obtained previously<sup>26</sup>. 42 T1 plants expressing *3SS::LFY<sub>K249R</sub>* were analyzed; the percentage of plants with a LFY overexpressing phenotype is comparable to the one obtained with *3SS::LFY*<sup>26</sup>. Source data are available in Supplementary Data 4.



Extended Data Fig. 9 | See next page for caption.

**Extended Data Fig. 9 | UFO binds DNA and LFY DBD.** **a**, A representative micrograph of the ASK1-UFO-LFY-DNA complex in vitreous ice (scale bar, 20 nm). **b**, Selected 2D class averages of the particles submitted to *ab initio* reconstruction and heterogeneous refinement for 3D classification. **c**, Intermediate reconstructions of the 3D classes after heterogeneous refinement. **d**, Final reconstructions of ASK1-UFO-LFY-DNA complexes (involving either a LFY-DBD monomer (pink) or a LFY-DBD dimer (gray)) after Non-Uniform refinement. **e**, Unprocessed AlphaFold2 model for ASK1 (top, purple; uniprot ID, Q39255), UFO (middle, red; uniprot ID, Q39090) and the LFY-DBD dimer/DNA crystallographic structure (bottom, pale and dark blue for

the LFY-DBD dimer and green for the DNA; PDB, 2VY1). **f**, Cryo-EM density map color-coded by fitted molecule. Note the kink on DNA induced by the presence of UFO. **g**, Heat map of the angular distribution of particle projections contributing for the final reconstruction of the complete ASK1-UFO-LFY-DNA complex (with a LFY-DBD dimer). **h**, Gold-standard Fourier shell correlation (FSC) curves. The dotted line represents the 0.143 FSC threshold, which indicates a nominal resolution of 6.4 Å for the unmasked (red) and 4.3 Å for the masked (blue) reconstruction. **i**, View of the post-processed map of the complete ASK1-UFO-LFY-DNA complex, colored according to the local resolution.

## Reporting Summary

Nature Portfolio wishes to improve the reproducibility of the work that we publish. This form provides structure for consistency and transparency in reporting. For further information on Nature Portfolio policies, see our [Editorial Policies](#) and the [Editorial Policy Checklist](#).

### Statistics

For all statistical analyses, confirm that the following items are present in the figure legend, table legend, main text, or Methods section.

n/a Confirmed

- The exact sample size ( $n$ ) for each experimental group/condition, given as a discrete number and unit of measurement
- A statement on whether measurements were taken from distinct samples or whether the same sample was measured repeatedly
- The statistical test(s) used AND whether they are one- or two-sided  
*Only common tests should be described solely by name; describe more complex techniques in the Methods section.*
- A description of all covariates tested
- A description of any assumptions or corrections, such as tests of normality and adjustment for multiple comparisons
- A full description of the statistical parameters including central tendency (e.g. means) or other basic estimates (e.g. regression coefficient) AND variation (e.g. standard deviation) or associated estimates of uncertainty (e.g. confidence intervals)
- For null hypothesis testing, the test statistic (e.g.  $F$ ,  $t$ ,  $r$ ) with confidence intervals, effect sizes, degrees of freedom and  $P$  value noted  
*Give P values as exact values whenever suitable.*
- For Bayesian analysis, information on the choice of priors and Markov chain Monte Carlo settings
- For hierarchical and complex designs, identification of the appropriate level for tests and full reporting of outcomes
- Estimates of effect sizes (e.g. Cohen's  $d$ , Pearson's  $r$ ), indicating how they were calculated

*Our web collection on [statistics for biologists](#) contains articles on many of the points above.*

### Software and code

Policy information about [availability of computer code](#)

Data collection	For DLRA: TECAN Spark 10M 96-well plate reader For EMSAs: Amersham ImageQuant 800 imager For Western Blots: ChemiDoc MP Imaging System For plant pictures: Keyence VHX-5000 microscope For SEC-MALLS: Dawn Heleos II for MALLS measurement (Wyatt Technology) and Optilab T-rEX refractometer for refractive index measurements (Wyatt Technology) For cryoEM: serialEM v3.8.17
Data analysis	Data analysis procedures are described in the Methods section. For DLRA: R studio v1.3.959 For SEC-MALLS: ASTRA v6.1.7.17 For cryoEM data analysis: cryoSPARC v3.0, crYOLO v1.7.6, DeepEMhancer, UCSF Chimera v1.15, UCSF ChimeraX v1.3 For cryoEM model building: Coot v0.9.7, UCSF Chimera v1.15, UCSF ChimeraX v1.3, PHENIX v1.20.1 Tools and versions used for bioinformatic analyses: fastqc v0.11.7 bowtie2 v2.3.4.1 NGmerge v0.2_dev MACS2 v2.2.7.1 bedtools v2.30.0 samtools v1.8 R 'plotROC' package v2.2.1

mspc v4.0.0  
R v3.5.0

For manuscripts utilizing custom algorithms or software that are central to the research but not yet described in published literature, software must be made available to editors and reviewers. We strongly encourage code deposition in a community repository (e.g. GitHub). See the Nature Portfolio [guidelines for submitting code & software](#) for further information.

## Data

Policy information about [availability of data](#)

All manuscripts must include a [data availability statement](#). This statement should provide the following information, where applicable:

- Accession codes, unique identifiers, or web links for publicly available datasets
- A description of any restrictions on data availability
- For clinical datasets or third party data, please ensure that the statement adheres to our [policy](#)

Data used in this study:

Microarray data: AtGenExpress (ATGE\_52A-C and ATGE\_29A-C)

LFY ampDAP-seq data: GSE160013

LFY ChIP-seq data: GSE141704, GSE96806, GSE64245, GSE24568

Structures: LFY-DBD dimer structure (RCSB PDB, 2VY1), Alphafold models of ASK1 (uniprot ID: Q39255) and UFO (uniprot ID: Q39090).

ampDAP-seq data have been deposited and are publicly available (GSE204796).

The cryo-EM structure determined in this study is deposited in the EM databank under the reference number EMD-15145.

Any additional information required to reanalyze the data reported in this paper is available from the lead contact upon request.

## Human research participants

Policy information about [studies involving human research participants and Sex and Gender in Research](#).

Reporting on sex and gender

N/A

Population characteristics

N/A

Recruitment

N/A

Ethics oversight

N/A

Note that full information on the approval of the study protocol must also be provided in the manuscript.

## Field-specific reporting

Please select the one below that is the best fit for your research. If you are not sure, read the appropriate sections before making your selection.

Life sciences

Behavioural & social sciences

Ecological, evolutionary & environmental sciences

For a reference copy of the document with all sections, see [nature.com/documents/nr-reporting-summary-flat.pdf](https://nature.com/documents/nr-reporting-summary-flat.pdf)

## Life sciences study design

All studies must disclose on these points even when the disclosure is negative.

Sample size

For DLRA, we followed standard practice for data replication and data analysis. Sample size was sufficient for statistical significance and reproducibility. For plant studies, we analyzed several independent lines as indicated in figure legends to minimize variability.

Data exclusions

No data excluded.

Replication

The number of replication for each experiment is indicated in Source data.  
GUS staining experiments were performed twice for all lines with similar results.  
ampDAP-seq was performed in triplicate or in duplicate as indicated in the Method section and was reproduced 3 times with similar results.

Randomization

For plant experiments, all T1 resistant plants were further analyzed without any selection criteria.

Blinding

Investigators performing the biochemical experiments also analyzed the data so blinding was not applied. For ampDAP-seq, libraries were analyzed without prior knowledge of the tested protein(s).

# Reporting for specific materials, systems and methods

We require information from authors about some types of materials, experimental systems and methods used in many studies. Here, indicate whether each material, system or method listed is relevant to your study. If you are not sure if a list item applies to your research, read the appropriate section before selecting a response.

## Materials & experimental systems

n/a	Involved in the study
<input type="checkbox"/>	<input checked="" type="checkbox"/> Antibodies
<input type="checkbox"/>	<input checked="" type="checkbox"/> Eukaryotic cell lines
<input checked="" type="checkbox"/>	<input type="checkbox"/> Palaeontology and archaeology
<input checked="" type="checkbox"/>	<input type="checkbox"/> Animals and other organisms
<input checked="" type="checkbox"/>	<input type="checkbox"/> Clinical data
<input checked="" type="checkbox"/>	<input type="checkbox"/> Dual use research of concern

## Methods

n/a	Involved in the study
<input checked="" type="checkbox"/>	<input type="checkbox"/> ChIP-seq
<input checked="" type="checkbox"/>	<input type="checkbox"/> Flow cytometry
<input checked="" type="checkbox"/>	<input type="checkbox"/> MRI-based neuroimaging

## Antibodies

### Antibodies used

HRP-conjugated anti-myc antibody (Invitrogen; Cat# R951-25; RRID:AB\_2314045) and HRP-conjugated anti-FLAG antibody (Sigma-Aldrich; Cat# A8592; RRID:AB\_439702).

### Validation

Provided by the supplier.

## Eukaryotic cell lines

Policy information about [cell lines](#) and [Sex and Gender in Research](#)

### Cell line source(s)

Sf21 insect cells.

### Authentication

None of the cell lines used were authenticated.

### Mycoplasma contamination

N/A

### Commonly misidentified lines (See [ICLAC](#) register)

N/A